HHS Public Access

Author manuscript

Nat Neurosci. Author manuscript; available in PMC 2018 May 15.

Published in final edited form as:

Nat Neurosci. 2017 November ; 20(11): 1580–1590. doi:10.1038/nn.4644.

Esr1+ cells in the ventromedial hypothalamus control female aggression

Koichi Hashikawa[1,*], **Yoshiko Hashikawa**[1,*], **Robin Tremblay**[1], **Jiaxing Zhang**[2], **James E. Feng**[1], **Alexander Sabol**[1], **Walter T. Piper**[3], **Hyosang Lee**[4], **Bernardo Rudy**[1], and **Dayu Lin**[1,3,5,6]

[1]Neuroscience Institute, New York University School of Medicine, 522 First Avenue, New York, NY 10016, USA

[2]Department of Physiology, Medical College of Xiamen University, 422 S Siming Rd, Xiamen, Fujian, 361005, China

[3]Center for Neural Science, New York University, 4 Washington Place, New York, NY 10003, USA

[4]Department of Brain and Cognitive Sciences, DGIST, Daegu, 42988, Korea

[5]Department of Psychiatry, New York University School of Medicine, 1 Park Avenue, New York, NY 10016, USA

[6]Emotional Brain Institute, New York University School of Medicine, 522 First Avenue, New York, NY 10016, USA

Summary

As an essential means to resolve conflicts, aggression is expressed by both sexes but often at a higher level in males than in females. Recent studies suggest that cells in the ventrolateral part of the ventromedial hypothalamus (VMHvl) that express estrogen receptor alpha and progesterone receptor (Esr1/PR) are essential for male but not female mouse aggression. In contrast, here we show an indispensable role of VMHvl^{Esr1+} cells in female aggression. This population is active when females attack naturally. Inactivation of these cells reduces female aggression whereas their activation elicits attack. Additionally, we found that female VMHvl contains two anatomically distinguishable subdivisions that show differential gene expression, projection and activation patterns after mating and fighting. These results support an essential role of the VMHvl in both

*These authors contributed equally to this work.

Assession codes

The RNAseq data is available from NIH GEO database:

Author Contributions

D. L. supervised the project. D.L. and K.H. conceptualized the project, designed experiments and wrote the manuscript. K.H. and Y. H. conducted most experiments and analyzed data. R. T. conducted *in vitro* slice physiology. J. Z. conducted pilot pharmacological and c-Fos experiments. J. E. F. optimized *in vivo* single unit recording. W.T.P. helped with pilot optogenetic experiments. A. S. helped with fiber photometry and optogenetic experiments. H. L. generated Esr1-2A-Cre mice. B. R. supervised slice physiology.

Competing Financial Interests Statement

The authors declare no competing financial interests

male and female aggression and reveal the existence of two previously unappreciated subdivisions in the female VMHvl that are involved in distinct social behaviors.

Introduction

Aggressive behavior is essential for competing for food, defending home, protecting self and family, and enhancing overall survival opportunity in both sexes. In many species, mating opportunities are limited and therefore aggression is also used to compete for mates. As a result of natural selection[1], males in those species often express higher level of aggression[2]. Given that aggressive behaviors are far more prevalent in males in many vertebrates, including humans, most studies of the biological basis of aggression have focused on males. Early lesion and electrical stimulation studies identified the medial hypothalamus as an essential region for male aggression[3–5]. Recently, studies from our group and others have identified the VMHvl, a small subnucleus situated most ventrally in the medial hypothalamus, as an essential region for male mouse aggression[6–11]. In particular, optogenetically activating the VMHvl cells expressing Esr1 (which overlaps nearly 100% with PR expression) elicited immediate attack whereas optogenetic inactivation of the VMHvl^{Esr1+} cells or ablation of the VMHvl^{PR+} cells abolished inter-male attack[6,9].

While one electrical stimulation study in rats suggested that male and female aggression involve similar medial hypothalamic regions[12], perturbing the VMHvl$^{Esr1+/PR+}$ cells appeared to affect only male but not female aggression[6,9]. In addition, male but not female aggression was reduced either by knocking out the Esr1 gene in the whole animal[13] or by suppressing its expression specifically in the VMHvl using RNAi[14,15]. Instead, the VMHvl has a well-established role in promoting female sexual behavior[9,16–19]. Electrical stimulation of the VMHvl can facilitate lordosis in female rats in the absence of males[19]. Most compellingly, Esr1 knockdown or ablating the VMHvl^{PR+} cells significantly reduced sexual receptivity but failed to reduce aggression in female mice[9,20]. These studies concluded that the Esr1/PR population in the VMHvl serves fundamentally different roles in female and male social behaviors – it mediates aggression in males but sexual behaviors in females[21–23].

Here, we re-examined the role of the VMHvl in female aggression using a series of functional manipulation and recording tools. We found clear evidence supporting an essential role of the VMHvl^{Esr1+} cells in female aggression. Additionally, we revealed two previously unappreciated subdivisions in the female VMHvl, one for aggression and one for sexual behaviors.

Results

Aggressive behaviors in laboratory female mice

Female aggression can differ widely based on females' reproductive state[24] and genetic background[25], and the opponent type[26]. Thus, we first tested the behaviors of laboratory female mice under a variety of resident-intruder conditions (Supplementary Table 1). We found that aggression can be reliably induced (defined as repeated attacks occurring in over 50 % of subject mice) when (1) a virgin SW female encountered a juvenile intruder (either

sex) in her home cage; (2) a lactating SW female encountered any intruder; or (3) a lactating C57 female encountered a juvenile intruder. We also noticed that some singly housed SW virgin female (6/10) briefly attacked a female intruder during initial encounter (latency to last attack: 68.7 ± 43.1 s). Unexpectedly, 6/10 singly housed C57 females showed male-style mounting towards female intruders and to a lesser extent, towards juveniles.

VMHvl^{Esr1+} cells are highly active during female aggression and sexual behaviors

Using the aggression-inducing conditions that we identified, we found that VMHvl consistently expressed high level of c-Fos, a surrogate marker of neural activity, after aggression in both virgin and lactating females (Supplementary Fig. 1). Importantly, the number of c-Fos$^+$ cells in the VMHvl was significantly larger in lactating females that attacked the adult male than those not, suggesting that VMHvl activation is at least partially due to the expression of aggression (Supplementary Fig. 1). Motivated by the high level of female aggression-induced c-Fos in the VMHvl, we pharmacogenetically inactivated the VMHvl in wild-type SW lactating females and found significantly reduced aggression, supporting an essential role of the VMHvl in female aggression (Supplementary Note 1 and Supplementary Fig. 2).

We next asked whether female aggression activated VMHvl cells are preferentially overlapped with the Esr1as previously observed in males[6]. Whereas approximately 50% of the VMHvl neurons expressed Esr1, 60–80% of fighting-induced c-Fos positive cells expressed Esr1 (Fig. 1a–c). This preferential overlap between Esr1 and fighting-induced c-Fos suggests that VMHvl^{Esr1+} cells may be a relevant population for female aggression. Consistent with a well-known role of the VMHvl cells, especially those express Esr1$^+$, in female sexual behaviors[9,16–20,27], mating induced abundant c-Fos expression in the VMHvl and over 90 % of c-Fos$^+$ cells expressed Esr1 (Fig. 1d).

To directly observe the activity of the VMHvl^{Esr1+} cells during female aggression and mating, we recorded the activity of VMHvl^{Esr1+} cells in freely-moving mice using fiber photometry[8,28,29] (Fig. 2a). We virally expressed a genetically encoded fluorescent calcium sensor, GCaMP6f[30], and a control fluorophore, mCherry, in the VMHvl of *Esr1-2A-Cre*[6] SW mice and implanted a 400 μm optic fiber above the injection site (Fig. 2b, c). Histological analysis revealed that 94.2 ± 2.0 % of cells under the light cone were within the VMHvl. During recording session, we sequentially introduced an adult male, a juvenile male, a pup or an object into the home cage of the recorded female in pseudo-randomized order, each for 15–20 minutes. During object investigation or general locomotion, the GCaMP6f signal did not change (Fig. 2d **and** Supplementary Movie 1). When the virgin female investigated or attacked a juvenile, or investigated or was mounted by a male, the GCaMP6f activity increased acutely and the response magnitudes during attack and mating were similar (Fig. 2e, f and j, Supplementary Movies 2–3). When the lactating female investigated or attacked a juvenile or a male intruder, GCaMP6f activity also increased. The magnitude of response during attacking adult males is higher than that during attacking juvenile males (Fig. 2g, h and k; Supplementary Movie 4; ΔF/F: attack juvenile, 8.0 ± 2.3 %; attack adult male, 15.1 ± 2.4 %, $p = 0.040$, paired t-test, N = 6). Activity change was minimal when the lactating female investigated or retrieved the pups (Fig. 2i). GCaMP6

signal also increased during investigation of urines. Adult male urine elicited larger responses than juvenile urine in lactating females but comparable responses in virgin females (Supplementary Fig. 3). Despite the clear VMHvl response to olfactory cues from the intruders, the signal increase during attack cannot be simply accounted by the olfactory inputs for two reasons. First, the GCaMP6f responses during attack-only trials (attack not followed or preceded by investigation) were significantly larger than the responses during investigation-only trials (investigation not followed or preceded by attack) (Fig. 2l). Second, GCaMP6 responses were similar during attack trials that were preceded by investigation and those that were not (attack with preceding investigation towards a juvenile in lactating females: 8.7 ± 2.7 %; attack only: 8.5 ± 2.6 %; p=0.88, paired *t-test*). Furthermore, we noticed that the responses during investigation were modulated by the level of aggression. The response during investigation was larger when it was followed by attack than when it was not (Fig. 2m). The response during investigation-only trials was significantly larger on attack days than no-attack days in virgin females (Fig. 2n).

In C57 female mice, qualitatively similar responses during investigation, mating and attack were observed (Supplementary Fig. 4). In all animals, the simultaneously-recorded mCherry signal was not significantly modulated during any of these behaviors (Fig. 2d–k, **red traces**; Supplementary Fig. 5). Together these data show that the VMHvl^{Esr1+} cells in females are highly active during aggression and sexual behaviors, but not maternal behaviors.

VMHvl^{Esr1+} cells are necessary for female aggression

To test the necessity of VMHvl^{Esr1+} cells for female aggression, we virally expressed hM4Di-mCherry in the VMHvl^{Esr1+} cells using *Esr1-2A-Cre* SW virgin female mice (Fig. 3a–b). For one group of animals, one week after viral injection, we paired each female with an adult male mouse until midterm pregnancy, and tested the animals between postpartum days 2–7. A second group of virgin females were not paired with males and tested three weeks after viral injection (Supplementary Fig. 6a–e).

During testing, we injected saline or clozapine-N-oxide (CNO, the engineered ligand of hM4Di)[31,32] intraperitoneally on interleaved days. *In vitro* whole-cell recordings from VMHvl brain slices confirmed that CNO suppressed the activity of hM4Di –mCherry expressing cells (Fig. 3c). Thirty minutes after i.p. injection, we introduced a male (for the lactating group) or a juvenile (for both lactating and virgin groups) into the home cage of the test animal for 10 min. CNO injection significantly and reproducibly reduced attack duration and frequency in the tested females regardless of their reproductive stage (Fig. 3d–g **and** Supplementary Fig. 6c–d). Social investigation, pup retrieval and locomotion were not affected by CNO injection (Fig. 3h–j; Supplementary Fig. 6e). The suppression of aggression was significantly correlated with the percentage of VMHvl cells expressing hM4Di-mCherry, such that animals with higher percentages of infected neurons showed more decrease in aggression after CNO injection (Fig. 3k). Control animals that expressed mCherry in the VMHvl^{Esr1+} cells showed no change in aggression after CNO injection (Fig. 3e–g, **black lines**).

Additionally, in lactating *Esr1-2A-Cre* mice with C57 background, inhibiting the VMHvl^{Esr1+} cells nearly abolished aggression against juvenile intruders (Supplementary

Fig. 6f–j). Thus, VMHvl^{Esr1+} cells are necessary for female aggression regardless of reproductive stage and genetic background.

VMHvl^{Esr1+} cells are sufficient for driving female aggression

We next tested the sufficiency of VMHvl^{Esr1+} cells in eliciting aggression in females by virally expressing ChR2-EYFP[33] in the VMHvl^{Esr1+} cells of *Esr1-2A-Cre* SW mice (Fig. 4a). Approximately 90% of ChR2-EYFP expressing cells were Esr1^{+} (Fig. 4b, c). We delivered blue light unilaterally to the VMHvl when the virgin female encountered an adult male or female intruder, two conditions with minimal natural aggression (Fig. 4d). Light induced increase in social investigation, attack or neither. Post-hoc histology revealed that attack and investigation were predominantly induced from stimulation sites that expressed more light-induced c-Fos in the posterior (Bregma: −1.6 to −2.0 mm) than the anterior VMHvl (Bregma: −1.4 mm) (Fig. 4e). Eight out of 12 posteriorly biased VMHvl sites (8 animals) elicited attack and all 12 sites elicited investigation. In contrast, none of the 6 anteriorly biased sites (4 animals) induced attack and only one site induced investigation (Fig. 4e, Supplementary Fig. 7). In those posterior VMHvl biased animals, low intensity light (20 ms, 20 Hz, 0.34 ± 0.078 mW) significantly increased only investigation (Fig. 4f–4g, Supplemental Movie 5), while higher intensity light (20 ms, 20 Hz, 1.86 ± 0.23 mW) elicited both investigation and attack (Fig. 4f, h, i **and** Supplemental Movie 5). Control SW females that expressed mCherry in the VMHvl^{Esr1+} cells showed no change in investigation or attack during light delivery (Fig. 4j).

One study showed optogenetic activation of VMHvl^{Esr1+} cells in C57 virgin females induced social investigation and mounting but not aggression[6]. We attempted to reconcile our results with the previous study by optogenetically activating the VMHvl^{Esr1+} cells in C57 females using the conditions identical to those for SW females. Consistent with the previous report[6], we observed light-induced social investigation and mounting but no attack (Supplementary Fig. 8a–e). The induced mounting was light-bounded and against both natural (e.g. female) and unnatural (e.g. male) social targets (Supplementary Fig. 8e; Supplementary movie 6). In support of a role of the female VMHvl in driving mounting, both c-Fos staining and fiber photometry recording revealed increased activity in the VMHvl due to natural female-female mounting (Supplementary Fig. 8f and 8g). In contrast to virgin C57 females, attack was induced from all stimulation sites (>10% light-induced c-Fos and posteriorly biased) in lactating C57 females that naturally attacked intruders (Supplementary Fig. 9; Supplementary movie 7). Previous studies implicated a correlation between the aggression level in lactating female rats and anxiety[34]. To test the possibility that our activation induced attack was due to change in anxiety, we activated the aggression-inducible VMHvl sites in an elevated plus maze and observed no significant differences in the amount of time animals spent in the open arm during pre-stimulation, light-on, sham-on and post-stimulation periods (Supplementary Fig. 10). Taken together, the VMHvl^{Esr1+} cells could drive both aggression and male-style mounting in female mice. The exact form of light-induced behavioral change follows the pattern of natural social behaviors which were determined by the animals' genetic background and reproductive state.

Distinct fighting and mating related cells in female VMHvl

The VMHvl^{Esr1+} cells are clearly essential for both female aggression and sexual behaviors[9,16–20,35]. How do the mating- and aggression-excited cells relate to each other? To address this question, we performed electrophysiological recordings in freely-moving virgin SW female mice[7,8,36,37]. A total of 103 single units were recorded from five females. Among them, 22 cells were juvenile-excited. They significantly increased firing rate during investigating and/or attacking a juvenile (Fig. 5a–c). The increase in firing is higher during attack than investigation (Fig. 5c). 27 cells were adult male-excited. They significantly increased firing rate during investigating an adult male and/or being mounted (Fig. 5d–f). Only 4 cells were excited by both males and juveniles. Additional 4 cells were suppressed during these interactions. As a population, the juvenile-excited cells did not change firing rate during male interaction and the male-excited cells were weakly suppressed during juvenile interaction (Supplementary Fig. 11a, b). Across all 103 cells, there was no correlation between the firing rate changes during attacking and mating (Fig. 5g), or during investigating juveniles and investigating males (Fig. 5h and Supplementary Fig. 11c) whereas the responses during investigating different strains of males or responses during investigating juvenile males and females were significantly correlated (Supplementary Fig. 11d, e). Thus, two largely distinct subpopulations, one for mating and one for fighting, exist in the female VMHvl.

In our five recorded animals, we noticed that the juvenile-excited and adult male-excited cells were not distributed evenly. In the animal with the most laterally positioned electrode bundle, only male-excited cells (8/11 recorded cells) were recorded. In contrast, only juvenile-excited cells (6/29 cells) were recorded from the animal with the most medially positioned electrode. In the remaining three animals with electrodes centrally located in the VMHvl, both juvenile- and male-excited cells were recorded (Fig. 5i).

Topographical organization of fighting and mating related cells in female VMHvl

To further understand the spatial distribution of fighting and mating related neurons in the VMHvl, we performed a side-by-side comparison of c-Fos induced by mating and fighting and noticed a clear difference. Fighting, regardless of the reproductive state of the female and the type of intruder, invariably induced dense c-Fos in the medial part of the VMHvl whereas the mating induced c-Fos$^+$ cells were more laterally located (Supplementary Fig. 12 a–c). To quantify this difference, we measured the position of each c-Fos$^+$ cell in the VMHvl and found that while fighting- and mating-induced c-Fos$^+$ cells were located at the similar medial-lateral level in the anterior VMHvl, the fighting-induced c-Fos were significantly more medially located than the mating-induced c-Fos in the posterior VMHvl (Supplementary Fig. 12a–c). Consistent with a more important role of the posterior VMHvl in female aggression, more c-Fos$^+$ cells were found at the posterior VMHvl than the anterior VMHvl after female aggression while c-Fos$^+$ cells induced by female mating were similarly distributed along the anterior-posterior axis (Supplementary Fig. 12d–e).

To compare the mating and fighting induced *c-fos* in the same animal, we used *c-fos* cellular compartment analysis of temporal activity by fluorescent *in situ* hybridization (catFISH)[7,38] and found that mating and fighting induced *c-fos* were clearly topographically organized

(Fig. 6a). Detailed cell counting revealed that in virgin females that experienced fighting or mating twice, approximately 70% of cells expressed both intranuclear and cytoplasmic *c-fos* at VMHvl (Fig. 6a, b). Lactating females that sequentially attacked an adult male and a juvenile intruder also showed high overlap between intranuclear and cytoplasmic *c-fos* (Fig. 6a, b). In contrast, when the female fought then mated, or mated then fought, only 10% of intranuclear and cytoplasmic *c-fos* overlapped (Fig. 6a, b; Supplemental Movie 8). These results indicate, first, that the same neurons are likely to be recruited during two successive episodes of the same social behavior, regardless of the type of intruder; and second, that female mating and fighting recruit largely distinct sets of neurons in spatially segregated regions of the VMHvl.

The female VMHvl contains two molecularly distinguishable subregions

The distinct c-Fos expression patterns after fighting and mating suggest that the female VMHvl may contain previously unappreciated compartments. We carefully examined the pan-neuronal staining and noticed a cell-poor region within the posterior VMHvl that readily separates the area into a medial and a lateral zone (VMHpvlm and VMHpvll) (Fig. 7a; Supplementary Fig. 13). Visualization of glutamatergic (*Vglut2-ires-Cre* × Ai6)[39,40] and GABAergic neurons (*Vgat-ires-Cre* × Ai6)[39,40] supported that the VMHpvlm/pvll were distinct from the surrounding nuclei, including tuberal nucleus and lateral hypothalamus. Whereas VMHvl surrounds contained dense GABAergic neurons as previously reported[41,42], VMHpvlm and VMHpvll were largely (>90%) occupied by glutamatergic neurons and $Esr1^+$ cells were nearly exclusively glutamatergic (Fig. 7b–c; Supplementary Fig. 13). As expected, the fighting-induced c-Fos was mainly in the VMHpvlm whereas the mating-induced c-Fos was mostly in the VMHpvll (Fig. 7d–e).

If the VMHpvll and VMHpvlm are distinct brain structures, they likely also differ in their gene expression pattern[43]. Indeed, we noticed that Esr1 was expressed in fewer cells and at a lower intensity in the VMHpvlm than in the VMHpvll (Esr1% in VMHpvlm: 39.9 ± 4.8%; VMHpvll: 68.5 ± 4.2%; $p = 0.0125$, N = 6 animals; average intensity of Esr1 staining of VMHpvll cells divided by that of VMHpvlm cells: 1.86 ± 0.24, $p = 0.037$, N = 4 animals, *t*-test). To understand the genetic differences between the VMHpvlm and VMHpvll comprehensively, we performed RNAseq using tissues dissected from VMHpvlm, VMHpvll, the anterior VMHvl (VMHavl), and dorsomedial VMH (VMHdm) from *Vglut2-ires-Cre* × Ai6 mice[44] (Fig. 7f, g). Principal component analysis revealed that samples from the same VMH region were clustered in the principal component space and apart from samples from other regions (Fig. 7h). 74 genes were found enriched in the VMHpvlm and 126 in the VMHpvll (Fig. 7i, Supplementary Dataset 1). Of note, while most VMHpvll-enriched genes expressed minimally in VMHdm (107/126, log2 ratio >1.2), only a small fraction of VMHpvlm-enriched genes were differentially expressed in the VMHdm (10/74, log2 ratio >1.2).

Consistent with the Esr1 staining results, the Esr1 mRNA had significantly higher copy number in the VMHpvll than the VMHpvlm ($p < 0.01$, Fig. 7i). We further validated the RNAseq results with *in situ* hybridization. Consistent with the RNAseq data, Cckar and Iigp1 were nearly exclusively expressed in the VMHpvll; Crhbp and Egflam were largely

confined in the VMHpvlm while Tac1 was expressed at high level in both VMHvl regions (Fig. 7j). These data support the existence of molecularly distinguishable medial and lateral subdivisions in the female posterior VMHvl.

Visualization of the downstream targets from the female VMHvl

Lastly, we investigated the projection patterns of the VMHpvll and VMHpvlm by stereotaxically injecting a small amount (15 nl) of AAV expressing CRE-dependent synaptophysin-mCherry[45] into the VMHvl of *Esr1-2A-CRE* virgin SW female mice (Fig. 8a–c; supplementary Fig. 14). 6 out of 21 injected animals showed clearly medially (N =2) or laterally (N =4) biased expression. In laterally but not medially biased animals, we noticed dense terminals in the anteroventral periventricular nucleus (AVPV) (Fig. 8d). To confirm this result, we injected fluorescence conjugated cholera toxin subunit B (CTB-555) into AVPV and found that retrogradely labeled cells were largely restricted in the VMHpvll (Fig. 8e–g). As a comparison, we injected CTB-555 into lateral PAG, a region that received comparable projection from the medially and laterally biased animals (Fig. 8d) and found the VMHpvlm and VMHpvll contained similar percentage of CTB-labeled cells (Fig. 8f, h). Interestingly, VMHvl cells retrogradely labeled from either AVPV or PAG overlapped highly with Esr1 (Fig. 8g; $CTB^{+}Esr1^{+}/CTB^{+}$%: from AVPV, 88.5 ± 1.4 %; from PAG, 84.1 ± 1.3 %; N = 3 animals). Finally, consistent with the fact that the AVPV was strongly innervated by mating-related VMHpvll but not by fighting-related VMHpvlm, we found that AVPV expressed high levels of *c-fos* after female mating but not fighting (Fig. 8i, j). In contrast, the number of fighting- and mating-induced *c-fos* cells was comparable in the lateral PAG (Fig. 8i, j).

Discussion

Our study identified the $VMHvl^{Esr1+}$ cells as the first neural population that is functionally essential and naturally active during female aggression (Supplementary Fig. 15a). Additionally, we found that while in the male VMHvl, the fighting and mating related cells overlap substantially[7,36], in the female VMHvl, mating and fighting each activates cells that are located in one of the two previously unrecognized subdivisions of the VMHvl (Supplementary Fig. 15b).

In two recent studies, the function of the $Esr1^{+}/PR^{+}$ VMHvl population in female aggression was examined along with its role in male aggression[6,9]. While both studies found a clear role of the $VMHvl^{Esr+/PR+}$ population in male aggression, its function in female aggression was unclear. Here, we optimized laboratory conditions under which female aggression could be reliably induced. We found that majority of singly housed SW virgin females readily attack juvenile intruders, making it possible to study female aggression beyond lactating period. In addition, by using acute reversible inhibition instead of permanent ablation[9], we minimized changes in female sexual behaviors and avoided possible long-term circuit compensation. We showed in four sets of experiments (Fig. 3, Supplementary Fig.2, 6) that VMHvl activity is necessary for female mouse aggression regardless of the reproductive stage or genetic background of the test females, or the intruder types. While the reproductive state, genetic

background, housing condition and social experience may fine tune the aggression circuit, the basic circuit wiring is likely to be stable.

Lee et. al. reported that attack was induced when they activated the VMHvl^{Esr1+} cells in C57 males but not virgin C57 females[6]. Here, we repeated this experiment and confirmed that activating the VMHvl^{Esr1+} cells in virgin C57 females did not induce attack but induced male-style mounting. In contrast, when the VMHvl was activated in the SW virgin females or C57 lactating females, immediate attack was induced. Noticeably, in all these optogenetic experiments, the light-induced behavior matched the natural behavior of the test animal: virgin C57 females mount female intruders and never attack any intruder whereas SW virgin females and lactating C57 females attack the intruders and never show any mounting (Supplementary Table 1). As shown by our c-Fos mapping and optical recording, the VMHvl is active during both male-style mounting and attack in females. Thus, we speculate that the VMHvl contains both populations essential for driving mounting and fighting in females and depending on the genetic background and reproductive state of the animals, one population is preferentially activated by the intruder to drive the corresponding behavior. Optogenetic stimulation reactivates the “dominant” VMHvl population and induces the dominant behavior at the time of stimulation. It is worth noting that male-style mounting behavior is commonly expressed by females in many species. It is believed to play a role in maintaining social dominance[46]. Thus, the mounting in C57 and attacking in SW may be considered as different actions for achieving the same goal. Whether it is a mere coincidence or by design that the VMHvl drives both dominance behaviors despite their different motor patterns remains to be elucidated by future studies.

Previous studies showed that low intensity activation of the VMHvl^{Esr1+} cells induces mounting and high intensity activation induces attack in males[6]. Here, we demonstrated that both mounting and attack can be induced in virgin female by activating the VMHvl^{Esr1+} population. Thus, the female VMHvl^{Esr1+} cells appear to have the capacity to mediate all the social functions ascribed to the corresponding population in males. In addition, the female VMHvl may contain a female-specific population that is specialized for female sexual behaviors (e.g., lordosis and ovulation). Our findings reveal that the VMHpvll is largely devoid of aggression-related cells and instead occupied by cells excited during female sexual behaviors. In contrast, the male VMHvl aggression-related and mating-related cells appear to occupy the entire medial-lateral span of the VMHvl (Supplementary Fig. 15c, d), leaving little room for cells designated for female-style sexual behavior. Consistent with this hypothesis, the VMHpvll-specific projection to the AVPV is largely absent in the male VMHvl[9] and the VMHpvll-specific gene, Cckar, is minimally expressed in the male VMHvl[47]. Perhaps, testosterone causes the expansion of the VMHpvlm and shrinkage of the VMHpvll during development and ultimately increases aggression and decreases female-style sexual behaviors in males.

While some social behaviors are qualitatively different between sexes in the sense that males and females express different patterns of consummatory acts, other behaviors may only differ quantitatively. Our results, consistent with previous studies[12,48–50], support common neural substrates for generating qualitatively similar behaviors in males and females whereas

sex-specific neural substrates are perhaps reserved for acts (e.g., ejaculation and nursing) unique to one sex.

Online Methods

Mice and housing

All procedures were approved by the NYULMC IACUC in compliance with the NIH guidelines for the care and use of laboratory animals. *Esr1-2A-Cre* knock-in mice[6] were provided by D. J. Anderson and are currently available from Jackson Laboratory (stock No. 017911). They were backcrossed to either SW or C57 for at least five generations. *Vgat-ires-Cre* and *Vglut2-ires-Cre* knock-in mice[39] were provided by B. Lowell and are now commercially available (Jackson Laboratory, stock No: 016962 and 016963). They were bred to SW background for over five generations. Ai6[40] was purchased from the Jackson Laboratory (Stock No.007906). Wild-type SW and C57 mice were purchased from Taconic and Charles River respectively. Mice were housed under a 12 h light-dark cycle (12 p.m. to 12 a.m. light), with food and water available *ad libitum*. All females were group-housed until adulthood. After surgery or one week before the resident-intruder test, the test females were singly housed unless they were paired with males or had a litter. Single housing is known to increase aggressiveness in female mice[51] and the reliable expression of aggression is essential for our *in vivo* recording, immediate early gene mapping and loss-of-function experiments.

Resident-intruder test

To explore behavioral conditions in which female mice show reliable aggression, we tested female aggression in various combinations of subject and intruder types. A juvenile male (C57, 16–25 days old), an adult male (C57, 2 months to 12 months, 18–25 g) or an adult female (C57, 2 months to 12 months, 18–25 g) intruder was introduced into the home cage of a singly housed virgin (2–4 months, SW and C57) or lactating (SW and C57, postpartum day 3–7, 3–5 months) female mouse for 15 minutes. All test females were singly house for at least one week. All intruder mice were group housed.

Immediate early gene mapping

To induce mating in females, a highly sexually experienced adult male intruder (C57, 4–18 months) was introduced into the home cage of a virgin test female (SW and C57, 2–4 months). Females were only included in the analysis if they showed receptive postures and their male partners achieved intromission. To induce aggression, we used the resident-intruder testing conditions that were effective in eliciting aggression in either virgin or lactating females. Only females attacked intruder for at least 5 episodes were included in the analysis. In control group, an object (toy mouse, Zanies) was introduced into the female's cage. To induce fighting and mating in males, an adult group housed C57 male (2–12 months) or a receptive C57 female (2–4 months) was introduced into the home cage of a singly-housed SW male (3–12 months, sexually experienced), respectively. Only males achieved intromission or attacked intruder for at least 5 episodes were included in the analysis. The receptivity of the female intruders was determined in advance by behavioral screening using a male mouse different from the testing mouse. For the c-Fos

immunostaining, each behavioral test lasted 15 minutes and the animals were perfused 90 minutes after the test. For catFISH, SW mice experienced two consecutive 5-minute behavioral episodes separated by 30 minutes and were sacrificed immediately after the termination of the second behavioral episode[7].

Video acquisition and behavioral analysis

Animal behaviors in functional manipulation experiments and fiber photometry experiments were video recorded from both the side and top of the cage using two synchronized cameras (Basler, acA640–100gm) and a commercial video acquisition software (StreamPix 5, Norpix) in a semi-dark room with infrared illumination at a frame rate of 25 frames/s. Manual behavioral annotation was performed on a frame-by-frame basis using custom software written in MATLAB (http://vision.ucsd.edu/~pdollar/toolbox/doc/index.html). Investigation was defined as active nose contact to any parts of the body of the intruder or an object by the resident mouse. Attacks were defined by a suite of actions initiated by the resident toward the intruder, which included pushes, lunges, bites, tumbling and fast locomotion episodes between such movements. Mounting refers to the period when the test female was on top of the intruder and held the intruder's lower back using her forelimbs. Being mounted was defined as the behavioral period when the adult male intruder mounted the test female[7].

Fiber photometry recording

The fiber photometry setup was constructed as previously described, with a few modifications[8,28]. A 390-Hz sinusoidal blue LED light (30 μW) (LED light: M470F1; LED driver: LEDD1B; both from Thorlabs) and a 150-Hz sinusoidal yellow LED light nm (30μW) (Thorlabs, M590F1) were bandpass filtered (passing band: 472 ± 15 nm, FF02-472/30-25; 590 ± 20 nm, FF01-590/20-25, Semrock) and delivered to the brain to excite GCaMP6f and mCherry, respectively. The emission lights traveling back through the same optic fiber, bandpass filtered (passing bands: 524 ± 29 nm and 628 ± 33 nm, FF01-524/628-25, Semrock) and detected by a Femtowatt Silicon Photoreceiver (Newport, 2151) and recorded using a real-time processor (RP2, Tucker Davis Technology (TDT)). The envelopes of the 390-Hz and 150-Hz signals reflected the respective intensity of the GCaMP and mCherry and were extracted in real time using a custom TDT program.

100 nl of AAV1-CAG-Flex-GCaMP6f (2.0×10^{12} vg/ml) (University of Pennsylvania vector core facility) was stereotactically injected into the unilateral VMHvl through a glass capillary using a Nanoinjector (World Precision Instruments, Nanoliter 2000) at 15 nl/min. Similar injection procedure was also used in all functional experiments. After injection, a custom-made optic fiber assembly (Thorlabs, BFH48-400 and CF440-10) was inserted ~100 μm above the VMHvl of *Esr1-2A-Cre* mice (2–4 months old) and was secured using dental cement (C&B Metabond, S380). The coordinates for targeting the VMHvl (Bregma AP: −1.7, ML: ± 0.67, DV:−5.68 mm) were determined based on a three dimensional fMRI mouse atlas[52]. To estimate the distribution of recorded cells, we analyzed the location of cells underneath the putative light core (angle = 28º) from the optic fiber (NA=0.48). All virgin mice were singly housed after the surgery and during the tests. For experiments using lactating females, female mice were paired with an adult male mouse a week after surgery

and were cohoused until midterm pregnancy. Pups were separated from lactating female mice 5 minutes before the tests.

The optical recording was performed 3–6 weeks after viral incubation. Prior to recording, pups, if any, were removed. During recording, a juvenile male (16 – 25 days), an adult C57 male (>2 months) and an object (toy mouse, Zanies) were introduced into the cage of the subject female mouse in a randomized order. Some animals were also tested with pups (Day 2 to 7) and adult female intruders (> 2 months). Each stimulus was presented for 15 to 20 minutes and at least twice. Five minutes intervals were given between each stimulus presentation. To examine neural response to olfactory cues from conspecifics (supplementary figure 3), urine from adult C57 males or juvenile males was collected onto the cotton tip and was presented in front of the nose of the subject female mice in their home cage for 4–6 times.

To account for the autofluorescence from the system and the brain, we measured fluorescent intensity of each mouse on the day after the surgery. This value was later subtracted from the GCaMP6 signal obtained during the actual experiments. The normalized fluorescent signals (Fn) during each stimulus presentation were obtained by dividing the adjusted raw GCaMP6 signal with the mean fluorescence value from −100 sec to 0 sec before the stimulus introduction. In Figure 2d (left), the subject's location was tracked using a custom-written Matlab program[7,53]. The velocity was calculated as the difference in animal's location between the current frame and the previous frame. The average GCaMP6f signal and the average velocity of each second throughout the recording were calculated to construct the scatter plot in Figure 2d. In Figure 2d–i, l–n, the onset/offset peri-event time histograms (PETHs) were constructed by first calculating the average raw GCaMP6 signal aligned to the onset/offset of the behavioral events, and then normalized by calculating $(F - F_{baseline})/F_{baseline}$. $F_{basline}$ was the average signal between −5 s and −3 s from the onset of the behavior. We did not use the period immediately before the behavioral onset as the baseline given that the GCaMP6 signal may start to increase prior to the behavioral onset. In Figure 2j–l,n, peak ΔF/F was defined as the maximum ΔF/F of the PETHs within 2 s after behavioral onset minus the maximum ΔF/F between −5 to −3 s before the behavioral onset. In Figure 2m, offset peak ΔF/F was defined as the maximum ΔF/F of the PETHs within 2 s before behavioral offset minus the maximum ΔF/F between −5 to −3 s before the behavioral onset.

hM4Di mediated neural silencing

For silencing VMHvl neurons in wildtype SW female mice (3–5 months), a mixture of AAV2-hSyn-DIO-hM4Di-mCherry (5.8×10^{12} vg/ml, UNC vector core) and AAV2-CMV-Cre (3.7×10^{13} vg/ml. University of Iowa vector core facility) in a 2:1 volume ratio was prepared. Control virus is a mixture of AAV2-hSyn-DIO-mCherry (2.0×10^{12} vg/ml. UNC vector core) and AAV2-CMV-Cre (3.7×10^{13} vg/ml. University of Iowa vector core facility) in a 2:1 volume ratio. Mice were bilaterally and stereotactically injected with a total of 350 nl of the mixed viruses each side. Seven days after the injection, each female mouse was paired with a male mouse until the female became visibly pregnant. From postpartum day 2 to day 7, mice in the test group were intraperitoneally injected with saline or CNO (0.5

mg/kg, Sigma, C0832) on interleaved days. Thirty minutes after injection, pups were removed from the female's cage and two minutes later a randomly selected group-housed adult C57 male intruder (18–25 g) was introduced for approximately ten minutes to evaluate the aggression level of the female. After the intruder mouse was removed from the cage, four pups were introduced into the furthest corner from the nest and the amount of time to retrieve all the pups back to the nest was recorded as an index of pup retrieval performance.

To silence the $Esr1^+$ population in VMHvl, we injected 140 nl/side of AAV1-Ef1α-DIO-hM4Di-mCherry (3.0×10^{12} vg/ml, UNC vector core) bilaterally into the VMHvl of *Esr1-2A-Cre* mice (either SW background or C57 background, 3–5 months). Control animals were of the same genetic background and were injected with 140 nl/side AAV2-hSyn-DIO-mCherry (3.0×10^{12} vg/ml. UNC vector core). Surgical and behavioral testing procedures were similar to those used for WT mice with three differences. First, both test and control animals received CNO and saline injections on interleaved days. Second, test animals were split into two groups. One group received saline injection on the first testing day and the second group received CNO injection on the first testing day. This counter-balanced procedure ensured that any observed changes in aggression were not due to natural fluctuation in aggression across postpartum days. Third, each female was tested first with a juvenile male mouse intruder (16–25 days) and then with an adult male mouse intruder. In addition to testing lactating subjects, the behavioral effects by silencing $Esr1^+$ population in the VMHvl of virgin female mice were also tested. Virgin SW *Esr1-2A-Cre* mice were injected with 140 nl/side of AAV1-Ef1α-DIO-hM4Di-mCherry (3.0×10^{12} vg/ml, UNC vector core) bilaterally into the VMHvl. Three weeks after the injection, they received saline and CNO (0.5 mg/kg, Sigma, C0832) on 6 interleaved days 30 minutes prior to the aggression test with a juvenile male intruder.

For behavioral analysis, all animals with >10% VMHvl cells expressing hM4Di-mCherry were included. To compare the aggression level after CNO and saline injections, data for each animal from all CNO injected days were combined, whereas data from all saline injected days were combined, given that no significant differences in behaviors were found across CNO days or across saline days. The shortest durations to retrieve all four pups among all saline days and among all CNO days were used for comparing the performance of pup retrieval. The correlation between the number of infected cells and the behavioral changes was examined using all animals with average attack duration on saline days over 20 s.

ChR2 mediated cell activation

For activating $VMHvl^{Esr1+}$ neurons, we stereotactically injected 100 nl of AAV2-Ef1α-DIO-ChR2-EYFP (2×10^{12} vg/ml, UNC vector core) bilaterally into the VMHvl of virgin SW or C57 *Esr1-2A-CRE* mice (3–5 months). The control females were injected with AAV2-hSyn-DIO-mCherry (3.0×10^{12} vg/ml, UNC vector core). Immediately after viral injection, a bilateral guide cannula (Plastics One, center-to-center distance: 1.5 mm) was inserted 0.7 mm above the target area and was secured using dental cement (C&B Metabond, S380).

After two weeks of viral incubation and on the test day, two 230 μm multimode optical fibers (Thorlabs) were inserted into the bilateral guide cannula (Plastics One) and secured

with a matching cap (Plastics one). The optic fiber ends were flushed with the cannula ends. Randomly selected group-housed adult C57 male or female mice (>2 months) were introduced into the subject's home cage, one at a time and each for 30–90 minutes. Blue light (473 nm, Shanghai Dream Laser) was delivered through the fiber unilaterally in 20 ms pulses at 20 Hz with the intensity ranging from 0.02 to 3 mW for 60 s. The light intensity was measured at the fiber end during pulsing using an optical power meter (Thorlabs, PM100D). Sham stimulation period (0 mW) was interleaved with the real light stimulation period as an internal control. All behavioral tests were repeated at least once to ensure the reproducibility of any light induced behavioral changes. Mice were killed within 30 days after viral injection so that ChR2-EYFP expressing cells can be counted. Overtime, EYFP expression increases in the membrane which makes the counting less reliable.

For activating $Esr1^{+}$ population in the VMHvl of *Esr1-2A-Cre* lactating mice with C57 background (3–5 months), 100 nl of AAV2-Ef1α-DIO-ChR2-EYFP (2×10^{12} vg/ml, UNC vector core) was bilaterally injected. One week after injection, each female was paired with an adult C57 male (3–12 months). Once the female became visibly pregnancy, the male was separated. On postpartum day 2, the lactating female was first tested in a resident-intruder assay against a juvenile intruder. If the female showed any attack, we then tested the light-induced behavioral change using the same stimulation protocol described above.

To confirm the efficacy of ChR2 stimulation in inducing neural activation, blue light (20 ms, 20 Hz, 1–2 mW, 7 times, 40-s on and 20-s off) was delivered in the absence of any intruder 90 minutes before killing the animals. The light intensity was the same as that optimized for eliciting attack on previous testing days. Non- attackers and control animals expressing only mCherry were stimulated with the same protocol at 1.5 mW. The neural activation was then assessed by c-Fos staining.

Tracing

To investigate downstream targets of $VMHvl^{Esr1+}$ cells, 15 nl of AAV9-Ef1α-DIO-synaptophysin-mCherry (1.0×10^{13} vg/ml, MIT viral core) was stereotactically injected unilaterally into the VMHvl of virgin *Esr1-2A-CRE* SW females (2–5 months). Four weeks after injection, animals were sacrificed for histological analysis. To label VMHvl neurons that project to AVPV or PAG, retrograde tracer choleratoxin subunit B conjugated to Alexa Fluor 488 or 555 (CTB-488 or CTB-555, 1mg/ml, ThermoFisher) was injected unilaterally into AVPV (0.07 mm, 0.1 mm, 4.75/5.05 mm; 60 nl of each site) or lateral PAG (0.25mm, −4.5mm, −1.9 mm and 0.29 mm, −4.8 mm, −1.8 mm; 80 nl of each site). Seven days after surgery, animals were sacrificed for histology analysis which includes Esr1 and fluorescent Nissl staining. As we observed no difference in the labeling pattern at the VMHvl between CTB-488 and CTB-555 injected animals, data from these two tracers were pooled for final analysis.

Immunohistochemistry

For detection of c-Fos and/or viral expression in WT mice, frozen sections were prepared. Animals were deeply anesthetized with a mixture of ketamine (100 mg/kg) and xylazine (10 mg/kg) and transcardially perfused with 20 ml of PBS, followed by 20 ml of 4%

paraformaldehyde (PFA, Sigma) in PBS. After perfusion, brains were harvested, soaked in 20 % of sucrose in PBS for 24 hours at 4 °C and then embedded with O.C.T compound (Fisher Healthcare). 25 μm (Fig. 1 and Supplementary Fig. 8, 10) or 35 μm (Supplementary Fig. 1–2) thick coronal brain sections were cut using a cryostat (Leica). Brain sections were washed with PBS (1×10 minutes) and PBST (0.1 % Triton X-100 in PBS, 1×10 minutes), blocked in 10 % normal donkey serum (NDS) in PBST for 30 minutes at room temperature (RT), and then incubated with primary antibodies in 1% NDS in PBST overnight at 4 °C. Sections were then washed with PBST (3×5 minutes), incubated with secondary antibodies in 1 % NDS in PBST for 2 h at RT, washed with PBST (2×10 minutes), counterstained with DAPI (Sigma), and finally washed again with PBS (2×10 minutes). Slides were coverslipped using mounting medium (VECTASHIELD, H1000).

For the experiments with the need to analyze Esr1 expression, fresh floating sections were prepared. Animals were deeply anesthetized with a mixture of ketamine (100 mg/kg) and xylazine (10 mg/kg) and transcardially perfused with 20 ml of PBS, followed by 40 ml of 4% PFA. Brains were post-fixed for 1–2 h in 4% PFA and transferred to PBS with 0.05 % sodium azide (Sigma) at 4 °C until sectioning. 40–60 μm thick coronal sections were obtained using a vibratome (Leica, VT1200). Sections were stored in PBS with 0.05 % sodium azide at 4 °C until use. Sections were washed with PBS (3×5 minutes) and then blocked in 10 % NDS in PBST (0.3 % Triton) for 2-h at RT, followed by incubation with primary antibodies in 10 % NDS in PBST (0.3 % Triton) for 72 h at 4 °C. Sections were washed with PBST (0.3 % triton, 3×30 minutes), incubated with secondary antibodies in 10 % NDS in PBST (0.3 % Triton) and NeuroTrace 435/455 Blue Fluorescent Nissl Stain (Life Technologies, 1:200) for 2 h at room temperature, washed with PBST (2×15 minutes) and PBS (2×15 minutes), mounted on slides and coverslipped with mounting medium.

The primary antibodies used were rabbit anti-Esr1 (1:500, Santa Cruz, sc-542, Lot #F1715. Unspecific staining was occasionally observed using other lots.), goat anti-c-Fos (1:200, Santa Cruz, sc52-g), rabbit anti-beta Galactosidase (1:500, Immunology Consultant Laboratory, RGAL-45A-Z) and mouse anti-NeuN (1:300, Millipore, MAB377). The secondary antibodies used were donkey anti-rabbit Alexa 488 (1:500, Life Technologies, A21206), donkey anti-rabbit Alexa 546 (1:500, Life Technologies, A10040), donkey anti-rabbit Alexa 594 (1:500, Life Technologies, A21207), donkey anti-goat Alexa 488 (1:500, Life Technologies, A11055), donkey anti-goat Alexa 594 (1:500, Life Technologies, A11058), donkey anti-goat Alexa 633 (1:500, Life Technologies, A21082) and donkey anti-goat CY5 (1:300, Jackson ImmunoResearch, 705-175-147).

Fluorescent in situ hybridization

For detecting *c-fos,* flash frozen sections were prepared. Briefly, mice were anesthetized immediately after the 5 minutes behavioral episode using isoflurane and decapitated. Brains were transferred to a beaker containing ice-chilled 2-Methylbutane (Sigma) and then the beaker was moved to dry ice-cold ethanol to quickly freeze the brains. The brains were frozen within 2 minutes after the termination of the behavior and then stored at −80 °C until sectioning.

Fluorescent in situ hybridization (FISH) was performed for detection of *c-fos*. As described previously[7], 2, 4-dinitrophenol (DNP)-labeled *c-fos* cRNA probe, and digoxigenin (DIG)-labeled *c-fos* intronic probe were synthesized using cDNAs with T7 polymerase (Roche). Hybridization was conducted with 1–2ng/μl cRNA probes at 56 °C for 16 h. Probe detection was performed using horseradish peroxidase-conjugated antibodies (PerkinElmer). Signals for DIG-labeled probes were further amplified using biotin-conjugated tyramide (PerkinElmer) that was subsequently visualized with Alexa 555-conjugated streptavidin (Life Technologies). Signals for DNP labeled probes were amplified using DNP-conjugated tyramide (PerkinElmer) that was subsequently detected with anti-DNP Alexa 488 (Life Technologies). Sections were counterstained with Hoechst (1:2000, Life Technologies).

For visualizing mRNAs except for *c-fos,* fixed sections were prepared. Mice were deeply anesthetized with a mixture of ketamine (100 mg/kg) and xylazine (10 mg/kg) and transcardially perfused with 20 ml of PBS, followed by 40 ml of 4% PFA in PBS. After perfusion, brains were harvested, soaked in 20 % of sucrose in PBS for 24 hours at 4 °C and then embedded with O.C.T compound. 20 μm thick coronal sections were obtained using a cryostat and mounted on slides. Slides were stored at −80 °C until use.

RNA probes for Tac1, Egflam, Crhbp, Cckar, and Iigp were designed following Allen Brain Atlas's probe design guideline (http://help.brain-map.org/display/mousebrain/Documentation?preview=/2818169/3276841/ABADataProductionProcesses.pdf). Briefly, transcript sequences of target genes were analyzed with BLAST and high homology regions were detected. Primers were designed with Primer-BLAST according to the guideline's criteria, avoiding the high homology region; primer size 20–24 nt; GC content 42–52%; final product size 300–1200 nt. DNA templates for riboprobe in vitro transcription were generated by PCR method using both cDNA clones and genomic DNA (Supplementary Dataset 2). For genomic DNA, nested-PCR was performed. For each target gene, 3–4 DIG-labeled probes were produced and mixed.

For genes except for c-fos, chromogenic in situ hybridization (CISH) was performed. Hybridization was performed with DIG-labeled riboprobes (1–2ng/μl) at 56 °C for 16 h. Probe detection was performed using horseradish peroxidase-conjugated antibodies (PerkinElmer). Signals for DIG-labeled probes were amplified using biotin-conjugated tyramide (PerkinElmer), followed by Streptavidin alkaline phosphatase reaction, and then detected by NBT (Nitro blue tetrazolium chloride, Sigma)/BCIP (5-Bromo-4-chloro-3-indolyl phosphate, and toluidine salt, Sigma).

Image acquisition

Tiled confocal images were acquired with 2 μm optical thickness using 20×, or 40× objectives (Zeiss LSM 510 or 700 microscope). The image acquisition settings were maintained for each experiment. Z-stacks were acquired for quantifying ChR2-EYFP and *c-fos* in catFISH experiments. Epifluorescent images were acquired for determining electrode location in Figure 5 (Zeiss Axio). Bright field images were acquired for CISH experiments in Figure 7 (Olympus AX70). ImageJ or Neurolucida (MBF Bioscience) were used to quantify the staining results by an observer blind to the experimental conditions.

Electrophysiological recordings of acute slices

A mixture of AAV1-Ef1α-DIO-hM4Di-mCherry (3.0×10^{12} vg/ml, UNC vector core) and AAV2-CMV-Cre (1.1×10^{14} vg/ml, University of Iowa vector core facility) was stereotactially injected into the VMHvl of virgin wildtype SW female mice (3–4 weeks). 100 nl of AAV1-Ef1α-DIO-hM4Di-mCherry (3.0×10^{12} vg/ml, UNC vector core) was stereotactially injected into the VMHvl of virgin Esr1-2A-CRE SW female mice (3–4 weeks). After 3 weeks of viral incubation, mice were anesthetized with intraperitoneal injection of pentobarbital (100 mg/kg body weight). Upon loss of reflexes, mice were transcardially perfused with ice-cold oxygenated ACSF containing the following (in mM): 87 NaCl, 75 sucrose, 2.5 KCl, 1.25 NaH_2PO_4, 26 $NaHCO_3$ 10 glucose, 1 $CaCl_2$ and 2 $MgCl_2$. Mice were then decapitated and 300 μm thick coronal slices were sectioned using a Leica VT-1200-S vibratome and incubated in a holding chamber at 32–35°C for 15–30 minutes followed by continued incubation at room temperature for at least 45–60 minutes before physiological recordings. A slice containing VMHvl was then transferred into a recording chamber submerged with oxygenated ACSF containing the following (in mM): 125 NaCl, 2.5 KCl, 1.25 NaH_2PO_4, 26 $NaHCO_3$, 10 glucose, 2 $CaCl_2$ and 1 $MgCl_2$ (pH = 7.4, bubbled with 95% O_2 and 5% CO_2), in addition to 10 μM CNQX, 25 μM AP-5 and 10 μM SR-95531 to block AMPA, NMDA and GABAA receptors, respectively. ACSF was perfused in the chamber (~5mL/minutes, 34°C) all throughout the experiment. Whole-cell current-clamp recordings were obtained from visually identified mCherry expressing cells using borosilicate pipettes (3–5 MΩ) containing the following (in mM): 130 K-gluconate, 6.3 KCl, 0.5 EGTA, 10 HEPES, 4 Mg-ATP, 0.3 Na-GTP (pH adjusted to 7.3 with KOH). Upon break-in, series resistance (typically 15–25 MΩ) was compensated and only stable recordings (<20% change) were included. Data were acquired using an Axopatch 700B amplifier, sampled at 20 kHz and filtered at 10 kHz. Since resting membrane potential was variable from cell to cell and some were spontaneously active, all cells were held at −60mV with a DC current and current steps protocols applied to extract basic sub- and suprathreshold electrophysiological properties such as input resistance and action-potential threshold. DC was then removed and 10 μM CNO was applied. After at least 5 minutes of CNO application, cells were held back at −60 mV and intrinsic properties were reassessed using the same protocols as before CNO application. Data were analyzed off-line using Clampfit 10.2 software (Molecular Devises).

In vivo electrophysiological recordings

The recording procedures were described previously[7]. Adult virgin SW females (3–6 months) are used for recording. The electrode is composed of sixteen 13-μm tungsten wires (California fine wires, part No M281770), each attached to a pin on a nanoconnector (Omnetics, No 1619). The electrode assemble is glued onto a movable aluminum block driven by a 00–90 screw (J.J. Morris) on a custom-made microdriver. Each turn of the screw advances the electrode by 280 μm. During surgery, three anchor screws (Part No. F000CE094) were drilled into the skull. The electrode was then lowered right above the VMHvl (Depth: 5.4 mm) and the microdriver was secured onto the skull and anchor screws using dental cement. After one week of recovery and on the day of recording, the electrode was connected to a chronic headstage (TDT, LP16CH) that was connected to a torqueless, feedback-controlled commutator (TDT, AC32). The headstage was further connected to a

16-channel preamplifier (TDT, RA16PA) and recorded with a real-time digital processor (TDT, RZ5). Signals from electrodes were band-pass filtered from 300 Hz to 3000 Hz. Each video frame acquisition was triggered by a TTL pulse from the recording setup to ensure synchronization between the video and the electrophysiological recording.

During recording, a juvenile male, a juvenile female, an adult C57male, an adult SW male or a toy mouse was introduced into the cage of the recorded female in a randomized order each for approximately 5 minutes and with 5 minutes in between. Each stimulus was introduced at least twice to test the reproducibility of cell responses. Each day, the entire recording was broken into 2–4 recording blocks, each for approximately 1 hour. The first 5 minutes of each block was used as the baseline period and no stimulus was presented during that period. After each recording session, the electrode bundle was advanced by 1/8 turn. After approximately 10 recording sessions in each subject, mice were killed and histological analyses were performed to verify the locations of the electrodes. Only animals with the successful targeting of the VHMvl were included in the final analysis.

Spike sorting was performed using Offline Sorter (Plexon). Individual units recorded from the same electrode were isolated using principal component analysis. Three criteria were imposed for identifying single units. 1) Signal to noise ratio was above 3; 2) The waveform of the spikes was stable in the entire recording session; 3) Spikes with inter-spike intervals below 3 ms were no more than 0.1 %. Only units meeting all three criteria were included in the final analysis. To analyze the firing rate during each behavior, we sequentially combined all the spikes occurred during a specific behavior and then calculated the number of spikes in each 1-s bin during the behavior. We then compared the firing rates during a behavior and that during the baseline period using t-test for each unit. Units were regarded as responsive to a social stimulus if: 1) The firing rate during investigation of a social stimulus was significantly higher than that during baseline (t-test, $p < 0.01$); 2) the significant response was repeatable. Across all 20 recording sessions, the duration of baseline is 448 ± 19.8 s. The durations of investigating a juvenile male and an adult C57 male are 111 ± 7.47 s and 65.2 ± 4.99 s, respectively.

We constructed the PETHs (±5s window, 250-ms bin) aligned to the onset of investigating or attacking a juvenile for juvenile-excited cell with at least 3s of each analyzed behavior. We constructed the PETHs aligned to the onset of investigating and being mounted by a male for adult male-excited cell with at least 3s of these two behaviors. 18 out of 22 juvenile-excited cells and 9/27 male-excited cells met these criteria and were used to construct the population PETHs in Figure 5b and 5e, respectively.

LCM-RNAseq

Three group housed adult *Vglut2-ires-cre × Ai6* female mice (10–12 weeks) were decapitated. The brains were flash frozen within 2 minutes and stored at −80 °C until sectioning. 20 μm thick coronal sections were obtained using a cryostat and mounted on slides that were dehydrated in 100% ETOH for 1 min and then dried by using a hair dryer. Slides were stored at −80 °C until use. Given that VMH is composed of largely glutamatergic cells that were surrounded by GABAergic cells and each subdivision of VMH has cell-poor boundary, the ZsGreen labeling in glutamatergic cells enabled recognition of

the subdivisions. The anterior one third of the VMHvl was regarded as VMHavl while the remaining VMHvl was regarded as posterior VMHvl. VMHdm, VMHavl, VMHpvlm and VMHpvll was laser-dissected using LMD6000 (Leica; a fluorescent microscope combined with a movable laser for microdissection). Collected tissues were lysed in extraction buffer and total RNA was isolated using PicoPure RNA isolation kit (ThermoFisher). The RNASeq libraries were then prepared using Clontech SMARTer® Stranded Total RNA-Seq Kit (Cat # 635006) and purified using AMPure beads (Beckman coulter). The quantity of the library was examined using Qubit RNA HS assay Kit (Thermo Fisher Scientific) and qPCR. The quality of the library was determined using Bioanalyzer (Agilent). Once the libraries were deemed as high quality (free of adapter dimers and in concentration >2 nM), we pooled 8 samples equimolarly and sequenced them on Illumina HiSeq 2500 using high output mode to achieve greater depth of coverage. Read alignment was carried out using HISAT2 (https://github.com/infphilo/hisat2) against the mouse mm10 reference genome obtained from ENSEMBL database (http://useast.ensembl.org/). The alignment results were then exported to an open source software— Featurecounts to determine the number of reads for each gene. Then, the Bioconductor software package DESeq2 was used to identify genes that were differentially expressed across VMH subregions (adjusted p value < 0.05). Among those significantly differentially expressed genes, we selected a subset of vlm and vll specific genes with moderate to high level of expression (vlm specific: vlm/vll >1.2 and vlm normalized counts > 4 at log2 scale; vll specific: vll/vlm >1.2 and vll normalized counts > 4 at log2 scale) and conducted *in situ* hybridization of each gene to visualize its expression pattern in the VMH.

Statistical analysis

Statistical analyses were performed using Matlab or Prism software (GraphPad). All statistical analyses were two-tailed. Comparisons between two groups were performed by unpaired or paired *t*-test. Comparisons among 3 or more groups were performed using ANOVA. Post hoc multiple comparisons were done using Holm-sidak test for paired data and Tukey test for unpaired data. All significant statistical results were indicated on the figures following the conventions: *p < 0.05, **p < 0.01, ***p < 0.001. Error bars represent ± s.e.m.

No statistical methods were used to predetermine the sample sizes, but our sample sizes are similar to those generally employed in the field. Data distribution was assumed to be normal but this was not formally tested. Cell count, anatomical and behavioral analysis were fully and/or partially conducted by experimenters blind to experimental conditions. A Life Sciences Reporting Summary is available.

Data availability

The data that support the findings of this study are available from the corresponding author upon reasonable request.

Code availability

The codes used to analyze data and generate figures in this study are available from the corresponding author upon reasonable request.

Supplementary Material

Refer to Web version on PubMed Central for supplementary material.

Acknowledgments

We thank D. Anderson for providing *Esr1-2A-Cre* mice and B. Lowell for providing V*glut2-ires-Cre, Vgat-ires-Cre* mice and AAV-DIO-synaptophysin-mCherry for the pilot experiments. We thank R. Machold and M. Baek for the technical supports on *in situ* hybridization and RNAseq, C. Loomis at NYULMC Experimental pathology research laboratory for help on laser capture microdissection, A. Heguy and Y. Zhang at NYULMC Genome technology center for help on RNAseq and T. Lhakhang at NYULMC Bioinformatics laboratory for help with sequence alignment. We thank A.L. Falkner, M. Halassa, G. Stuber and G. Suh for critical comments on the manuscript. This research was supported JSPS oversea fellowship (K.H.), Uehara postdoctoral fellowship (K. H.), National Natural Science Foundation of China 81471630 (J.Z.), 1K99NS074077 (NIH) (H. L.), NIH R21NS093987 (B.R.), P01NS074972 (B.R.), NIH 1R01MH101377 (D. L.), NIH 1R21MH105774-01A1 (D. L.), Mathers foundation (D. L.), Irma T. Hirschl Career Scientist Award (D. L.), Sloan Research Fellowship (D. L.), McKnight Scholar Award (D. L.), Whitehall Fellowship (D. L.) and Klingenstein Fellowship Award (D.L.).

References

1. Darwin, C. The descent of man, and selection in relation to sex. D. Appleton and company; 1871.
2. Lindenfors P, Tullberg BS. Evolutionary aspects of aggression the importance of sexual selection. Adv Genet. 2011; 75:7–22. DOI: 10.1016/B978-0-12-380858-5.00009-5 [PubMed: 22078475]
3. Kruk MR, et al. Discriminant analysis of the localization of aggression-inducing electrode placements in the hypothalamus of male rats. Brain Res. 1983; 260:61–79. [PubMed: 6681724]
4. Olivier B, Wiepkema PR. Behaviour changes in mice following electrolytic lesions in the median hypothalamus. Brain Res. 1974; 65:521–524. [PubMed: 4472010]
5. Siegel A, Roeling TAP, Gregg TR, Kruk MR. Neuropharmacology of brain-stimulation-evoked aggression. Neurosci Biobehav R. 1999; 23:359–389.
6. Lee H, et al. Scalable control of mounting and attack by Esr1+ neurons in the ventromedial hypothalamus. Nature. 2014; 509:627–632. doi:nature13169 [pii] 10.1038/nature13169. [PubMed: 24739975]
7. Lin D, et al. Functional identification of an aggression locus in the mouse hypothalamus. Nature. 2011; 470:221–226. doi:nature09736 [pii] 10.1038/nature09736. [PubMed: 21307935]
8. Falkner AL, Grosenick L, Davidson TJ, Deisseroth K, Lin D. Hypothalamic control of male aggression-seeking behavior. Nat Neurosci. 2016
9. Yang CF, et al. Sexually dimorphic neurons in the ventromedial hypothalamus govern mating in both sexes and aggression in males. Cell. 2013; 153:896–909. DOI: 10.1016/j.cell.2013.04.017 [PubMed: 23663785]
10. Falkner AL, Dollar P, Perona P, Anderson DJ, Lin D. Decoding ventromedial hypothalamic neural activity during male mouse aggression. J Neurosci. 2014; 34:5971–5984. doi:34/17/5971 [pii] 10.1523/JNEUROSCI.5109-13.2014. [PubMed: 24760856]
11. Falkner AL, Lin D. Recent advances in understanding the role of the hypothalamic circuit during aggression. Front Syst Neurosci. 2014; 8:168. [PubMed: 25309351]
12. Kruk MR, et al. Comparison of aggressive behaviour induced by electrical stimulation in the hypothalamus of male and female rats. Prog Brain Res. 1984; 61:303–314. doi:S0079-6123(08)64443-X [pii] 10.1016/S0079-6123(08)64443-X. [PubMed: 6543251]
13. Ogawa S, Lubahn DB, Korach KS, Pfaff DW. Behavioral effects of estrogen receptor gene disruption in male mice. Proc Natl Acad Sci U S A. 1997; 94:1476–1481. [PubMed: 9037078]
14. Spiteri T, et al. The role of the estrogen receptor alpha in the medial amygdala and ventromedial nucleus of the hypothalamus in social recognition, anxiety and aggression. Behav Brain Res. 2010; 210:211–220. DOI: 10.1016/j.bbr.2010.02.033 [PubMed: 20184922]
15. Sano K, Tsuda MC, Musatov S, Sakamoto T, Ogawa S. Differential effects of site-specific knockdown of estrogen receptor α in the medial amygdala, medial pre-optic area, and

ventromedial nucleus of the hypothalamus on sexual and aggressive behavior of male mice. Eur J Neurosci. 2013; 37:1308–1319. DOI: 10.1111/ejn.12131 [PubMed: 23347260]

16. Aou S, Oomura Y, Yoshimatsu H. Neuron activity of the ventromedial hypothalamus and the medial preoptic area of the female monkey during sexual behavior. Brain Res. 1988; 455:65–71. [PubMed: 3416194]
17. Oomura Y, Aou S, Koyama Y, Fujita I, Yoshimatsu H. Central control of sexual behavior. Brain Res Bull. 1988; 20:863–870. [PubMed: 3409059]
18. Pfaff DW, Sakuma Y. Deficit in the lordosis reflex of female rats caused by lesions in the ventromedial nucleus of the hypothalamus. J Physiol. 1979; 288:203–210. [PubMed: 469716]
19. Pfaff DW, Sakuma Y. Facilitation of the lordosis reflex of female rats from the ventromedial nucleus of the hypothalamus. J Physiol. 1979; 288:189–202. [PubMed: 469715]
20. Musatov S, Chen W, Pfaff DW, Kaplitt MG, Ogawa S. RNAi-mediated silencing of estrogen receptor {alpha} in the ventromedial nucleus of hypothalamus abolishes female sexual behaviors. Proc Natl Acad Sci U S A. 2006; 103:10456–10460. doi:0603045103 [pii] 10.1073/pnas.0603045103. [PubMed: 16803960]
21. Yang CF, Shah NM. Representing sex in the brain, one module at a time. Neuron. 2014; 82:261–278. DOI: 10.1016/j.neuron.2014.03.029 [PubMed: 24742456]
22. Bayless DW, Shah NM. Genetic dissection of neural circuits underlying sexually dimorphic social behaviours. Philos Trans R Soc Lond B Biol Sci. 2016; 371:20150109. [PubMed: 26833830]
23. Yang T, Shah NM. Molecular and neural control of sexually dimorphic social behaviors. Curr Opin Neurobiol. 2016; 38:89–95. DOI: 10.1016/j.conb.2016.04.015 [PubMed: 27162162]
24. Lonstein JS, Gammie SC. Sensory, hormonal, and neural control of maternal aggression in laboratory rodents. Neurosci Biobehav Rev. 2002; 26:869–888. doi:S0149763402000878 [pii]. [PubMed: 12667494]
25. Parmigiani S, Palanza P, Rogers J, Ferrari PF. Selection, evolution of behavior and animal models in behavioral neuroscience. Neurosci Biobehav Rev. 1999; 23:957–969. [PubMed: 10580310]
26. Hurst JL, Barnard CJ. Kinship and Social Tolerance among Female and Juvenile Wild House Mice - Kin Bias but Not Kin Discrimination. Behav Ecol Sociobiol. 1995; 36:333–342. DOI: 10.1007/Bf00167794
27. Koyama Y, Fujita I, Aou S, Oomura Y. Proceptive presenting elicited by electrical stimulation of the female monkey hypothalamus. Brain Res. 1988; 446:199–203. [PubMed: 3285963]
28. Gunaydin LA, et al. Natural neural projection dynamics underlying social behavior. Cell. 2014; 157:1535–1551. DOI: 10.1016/j.cell.2014.05.017 [PubMed: 24949967]
29. Cui G, et al. Concurrent activation of striatal direct and indirect pathways during action initiation. Nature. 2013; 494:238–242. doi:nature11846 [pii] 10.1038/nature11846. [PubMed: 23354054]
30. Chen TW, et al. Ultrasensitive fluorescent proteins for imaging neuronal activity. Nature. 2013; 499:295–300. DOI: 10.1038/nature12354 [PubMed: 23868258]
31. Armbruster BN, Li X, Pausch MH, Herlitze S, Roth BL. Evolving the lock to fit the key to create a family of G protein-coupled receptors potently activated by an inert ligand. Proc Natl Acad Sci U S A. 2007; 104:5163–5168. DOI: 10.1073/pnas.0700293104 [PubMed: 17360345]
32. Dong S, Rogan SC, Roth BL. Directed molecular evolution of DREADDs: a generic approach to creating next-generation RASSLs. Nat Protoc. 2010; 5:561–573. doi:nprot.2009.239 [pii] 10.1038/nprot.2009.239. [PubMed: 20203671]
33. Boyden ES, Zhang F, Bamberg E, Nagel G, Deisseroth K. Millisecond-timescale, genetically targeted optical control of neural activity. Nat Neurosci. 2005; 8:1263–1268. doi:nn1525 [pii] 10.1038/nn1525. [PubMed: 16116447]
34. Bosch OJ, Meddle SL, Beiderbeck DI, Douglas AJ, Neumann ID. Brain oxytocin correlates with maternal aggression: link to anxiety. J Neurosci. 2005; 25:6807–6815. DOI: 10.1523/JNEUROSCI.1342-05.2005 [PubMed: 16033890]
35. Nomoto K, Lima SQ. Enhanced male-evoked responses in the ventromedial hypothalamus of sexually receptive female mice. Curr Biol. 2015; 25:589–594. DOI: 10.1016/j.cub.2014.12.048 [PubMed: 25683805]

36. Wong LC, et al. Effective Modulation of Male Aggression through Lateral Septum to Medial Hypothalamus Projection. Curr Biol. 2016; 26:593–604. DOI: 10.1016/j.cub.2015.12.065 [PubMed: 26877081]
37. Falkner AL, Dollar P, Perona P, Anderson DJ, Lin D. Decoding ventromedial hypothalamic neural activity during male mouse aggression. J Neurosci. 2014; 34:5971–5984. DOI: 10.1523/JNEUROSCI.5109-13.2014 [PubMed: 24760856]
38. Guzowski JF, McNaughton BL, Barnes CA, Worley PF. Environment-specific expression of the immediate-early gene Arc in hippocampal neuronal ensembles. Nat Neurosci. 1999; 2:1120–1124. DOI: 10.1038/16046 [PubMed: 10570490]
39. Vong L, et al. Leptin action on GABAergic neurons prevents obesity and reduces inhibitory tone to POMC neurons. Neuron. 2011; 71:142–154. DOI: 10.1016/j.neuron.2011.05.028 [PubMed: 21745644]
40. Madisen L, et al. A robust and high-throughput Cre reporting and characterization system for the whole mouse brain. Nat Neurosci. 2010; 13:133–140. DOI: 10.1038/nn.2467 [PubMed: 20023653]
41. Sapin E, et al. A very large number of GABAergic neurons are activated in the tuberal hypothalamus during paradoxical (REM) sleep hypersomnia. PLoS One. 2010; 5:e11766. [PubMed: 20668680]
42. Jennings JH, et al. Visualizing hypothalamic network dynamics for appetitive and consummatory behaviors. Cell. 2015; 160:516–527. doi:S0092-8674(14)01632-8 [pii] 10.1016/j.cell.2014.12.026. [PubMed: 25635459]
43. Lein ES, et al. Genome-wide atlas of gene expression in the adult mouse brain. Nature. 2007; 445:168–176. DOI: 10.1038/nature05453 [PubMed: 17151600]
44. Espina V, Milia J, Wu G, Cowherd S, Liotta LA. Laser capture microdissection. Methods in molecular biology. 2006; 319:213–229. DOI: 10.1007/978-1-59259-993-6_10 [PubMed: 16719357]
45. Garfield AS, et al. A neural basis for melanocortin-4 receptor-regulated appetite. Nat Neurosci. 2015; 18:863–871. DOI: 10.1038/nn.4011 [PubMed: 25915476]
46. Fang J, Clemens LG. Contextual determinants of female-female mounting in laboratory rats. Anim Behav. 1999; 57:545–555. DOI: 10.1006/anbe.1998.1025 [PubMed: 10196044]
47. Xu X, et al. Modular genetic control of sexually dimorphic behaviors. Cell. 2012; 148:596–607. DOI: 10.1016/j.cell.2011.12.018 [PubMed: 22304924]
48. Unger EK, et al. Medial amygdalar aromatase neurons regulate aggression in both sexes. Cell Rep. 2015; 10:453–462. DOI: 10.1016/j.celrep.2014.12.040 [PubMed: 25620703]
49. Wu Z, Autry AE, Bergan JF, Watabe-Uchida M, Dulac CG. Galanin neurons in the medial preoptic area govern parental behaviour. Nature. 2014; 509:325–330. DOI: 10.1038/nature13307 [PubMed: 24828191]
50. Kimchi T, Xu J, Dulac C. A functional circuit underlying male sexual behaviour in the female mouse brain. Nature. 2007; 448:1009–1014. DOI: 10.1038/nature06089 [PubMed: 17676034]
51. Kuchiiwa S, Kuchiiwa T. A novel semi-automated apparatus for measurement of aggressive biting behavior in mice. J Neurosci Methods. 2014; 228:27–34. DOI: 10.1016/j.jneumeth.2014.02.017 [PubMed: 24631320]
52. Chan E, Kovacevic N, Ho SK, Henkelman RM, Henderson JT. Development of a high resolution three-dimensional surgical atlas of the murine head for strains 129S1/SvImJ and C57Bl/6J using magnetic resonance imaging and micro-computed tomography. Neuroscience. 2007; 144:604–615. DOI: 10.1016/j.neuroscience.2006.08.080 [PubMed: 17101233]
53. Wang L, Chen IZ, Lin D. Collateral pathways from the ventromedial hypothalamus mediate defensive behaviors. Neuron. 2015; 85:1344–1358. DOI: 10.1016/j.neuron.2014.12.025 [PubMed: 25754823]

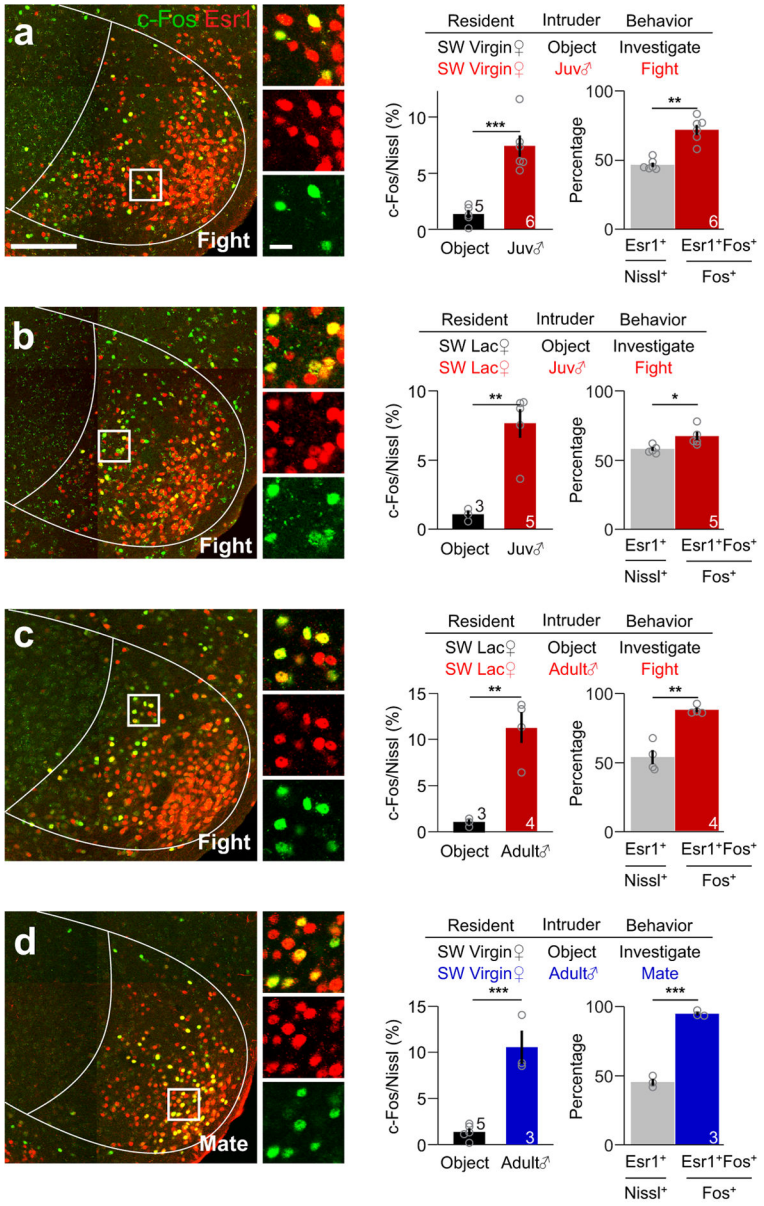

Figure 1. Esr1^{+} neurons in the VMHvl of female mice are preferentially activated during fighting and mating

(a–d) left: Representative images showing the expression of Esr1 (red) and c-Fos (green) in the VMHvl of **(a)** a virgin or **(b)** a lactating female mouse that attacked a juvenile male mouse, **(c)** a lactating female mouse that attacked an adult male mouse and **(d)** a virgin female mouse that mated with an adult male. Insets show the boxed areas. Scale bars: 150 μm and 20 μm (insets). Middle: The percentage of neurons in the VMHvl that expressed c-Fos after various stimulus conditions. Unpaired *t*-test. Right: The percentage of Esr1^{+} neurons in all VMHvl neurons (gray) and the percentage of c-Fos^{+} neurons expressing Esr1 in the VMHvl after fighting (red) or mating (blue). Paired *t*-test. $^{*}p < 0.05$, $^{**}p < 0.01$, $^{***}p < 0.001$. Data are presented as means ± s.e.m. The N for each group is indicated on the bar..

[AU Query: OK?] See Supplementary Table 2 for detailed statistics. **See also** Supplementary Figure 1.

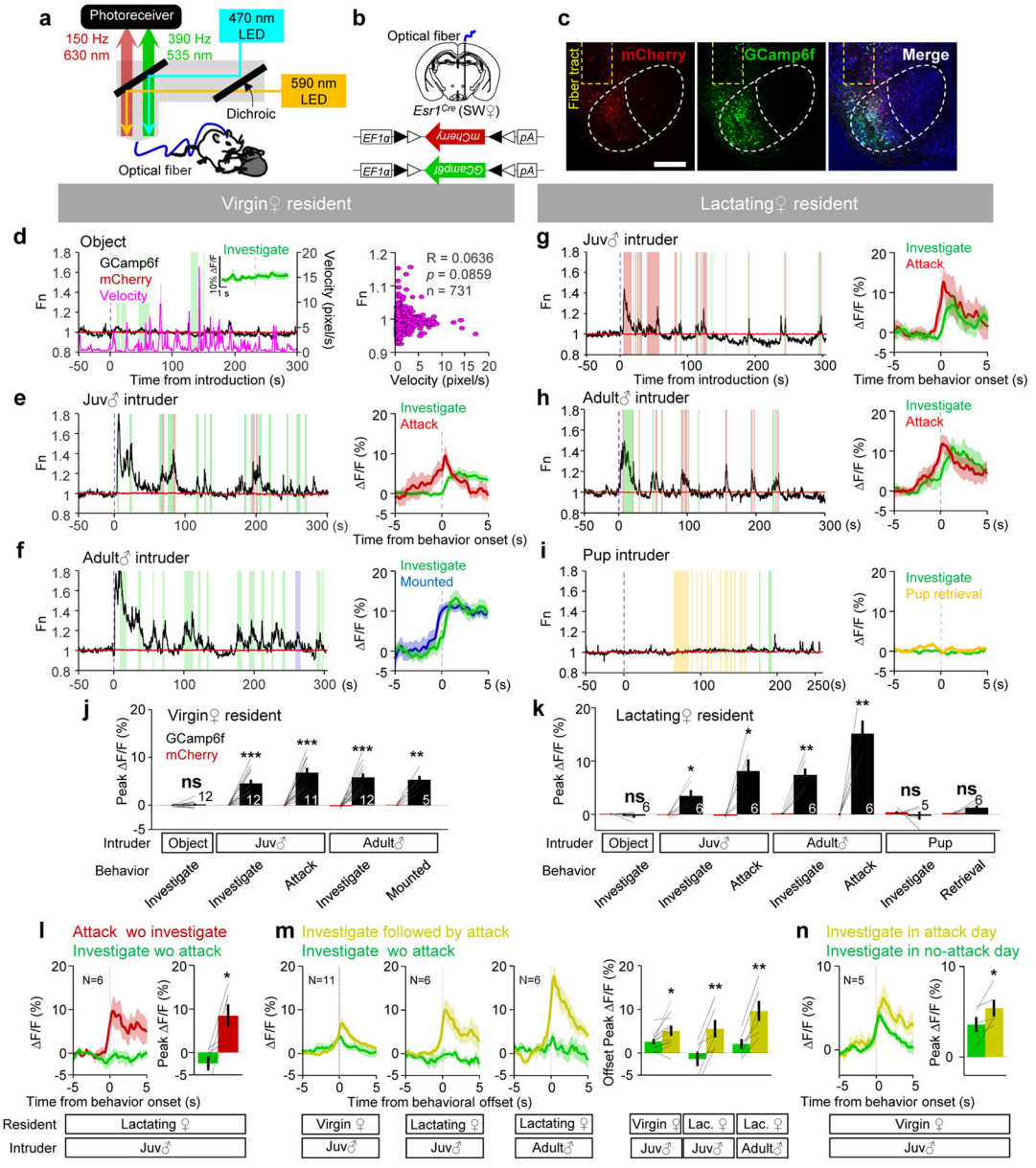

Figure 2. Responses of Esr1^{+} population in the female VMHvl during fighting and mating

(a) Light paths of the fiber photometry recording setup. **(b)** Viral constructs and implantation scheme. **(c)** Representative images showing mCherry (red), GCaMP6f (green), Nissl (blue) and optical fiber tract (yellow dashed line). Scale bar: 300 μm. **(d–i)** (left): Representative normalized GCaMP6f (black) and mCherry (red) traces during interaction with (**d**) an object and (**e–i**) various social stimuli introduced into the home cage of the test female. Colored shades mark behavioral episodes. Green: investigation; Blue: mounted; Red: attack, Yellow: pup retrieval. **(d)** (right): The velocity of the recorded animal did not correlate with GCaMP6f signal. Pearson product-moment correlation. Inset in **(d)** and right panels in **(e–i)** showing representative PETHs of GCaMP6f signal aligned to the onset of various behaviors. **(j–k)** The peak ΔF/F of GCaMP6f (black) and mCherry (red) signals during various

behaviors in virgin (**j**) and lactating (**k**) females. **(l–n)** Population PETHs (left) and the peak ΔF/F (right) of GCaMP6f signals aligned to the onset (**l, n**) or offset (**m**) of various behaviors. **j, k, l, m and n:** paired *t*-test. $^{*}p < 0.05$, $^{**}p < 0.01$, $^{***}p < 0.01$. Data are presented as means ± s.e.m.. [AU Query: OK?] See Supplementary Table 2 for detailed statistics. **See also** Supplementary Figure 3–5.

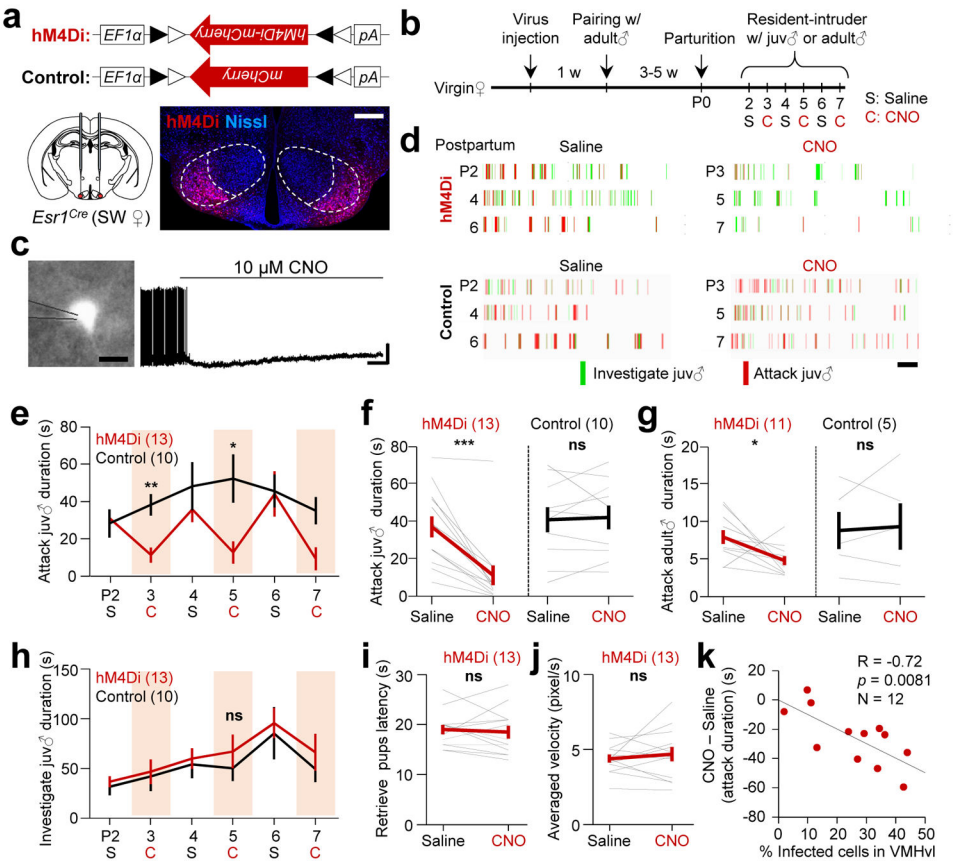

Figure 3. The activity of Esr1^{+} neurons in the VMHvl is necessary for female aggression

(a) Viral constructs and a representative histological image showing the expression of hM4Di-mCherry (red) at the injection sites. Scale bar: 300 μm. **(b)** Experimental schedule. **(c)** *In vitro* whole-cell patch clamp recording from a representative Esr1^{+} neuron in the VMHvl (Left, scale bar: 10 μm). Right shows changes in the cell's spontaneous spiking activity after 10 μM CNO application. Horizontal and vertical scale bars: 30 s and 20 mV. The result was replicated in two hM4Di-mCherry expressing cells. **(d)** Behavioral results of representative test and control animals. Scale bar: 60 s. **(e)** Reduction in aggression was reproduced in multiple CNO injected days. **(f, g)** Attack durations towards **(f)** juvenile male and **(g)** adult male intruders were significantly decreased after CNO injection in hM4Di group but not in control group. **(h–j)** No significant change was observed in **(h)** duration of investigation of a juvenile male intruder, **(i)** the time spent to retrieve four scattered pups and **(j)** the average movement velocity in the hM4Di group after CNO injection in comparison to saline injection. **e–j** only include animals with over 10% of infected cells in the VMHvl. (**k**) The percentage of cells that were infected in the VMHvl was significantly correlated with the amount of decrease in attack duration towards a juvenile male intruder after CNO injection. **k** includes all animals with attack duration over 20 s on saline days regardless of the percentage of infected cells. **e and h:** Two-way repeated measure ANOVA followed by Holm-Sidak post-hoc multiple comparisons; **f, g, i and j**: Paired *t*-test; **k:** Pearson product-moment correlation. $^{*}p < 0.05$, $^{**}p < 0.01$, $^{***}p < 0.001$. Data are presented as means ±

s.e.m.. [AU Query: OK?] See Supplementary Table 2 for detailed statistics. **See also** Supplementary Figure 6.

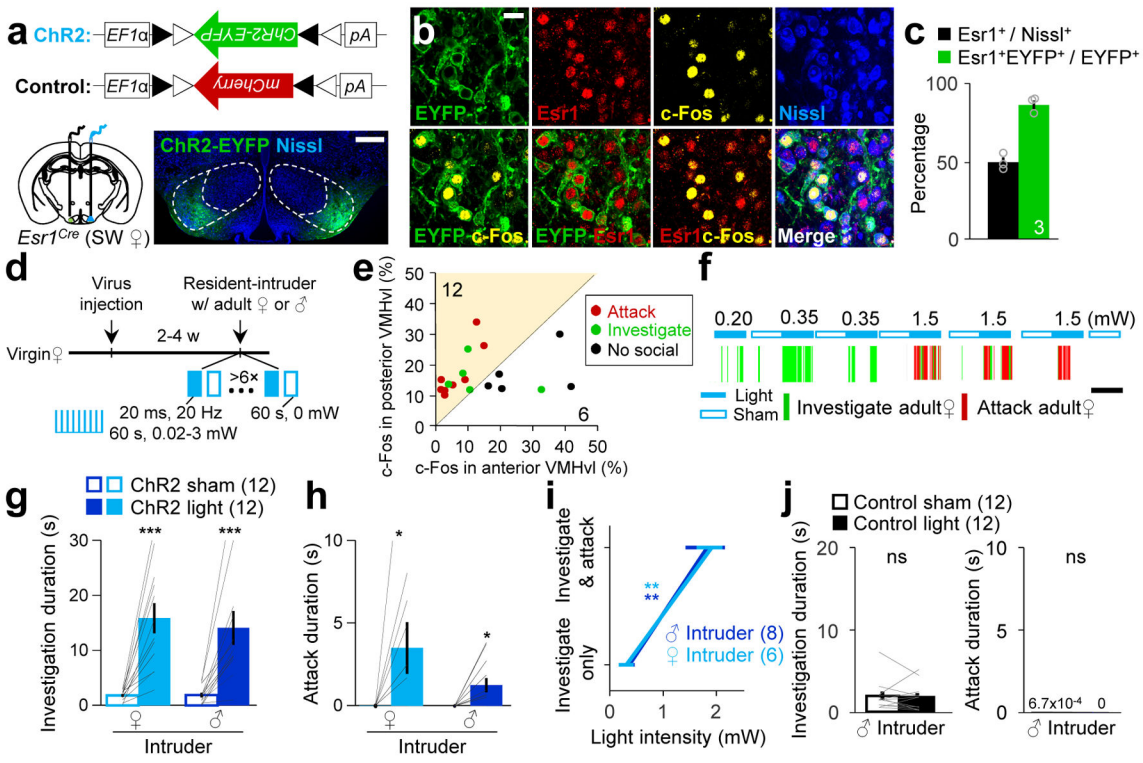

Figure 4. Activation of the Esr1^{+} neurons in the VMHvl is sufficient to induce attack in virgin female mice

(a) Viral constructs and a histological picture showing the ChR2-EYFP expression (green) at the injection sites. Scale bar: 300 μm. **(b)** Images showing the expressions of ChR2-EYFP (green), Esr1 (red), c-Fos (yellow), Nissl (blue) and their overlaps. Scale bar: 20 μm. **(c)** The percentage of all VMHvl neurons expressing Esr1 (black) and the percentage of ChR2-EYFP^{+} neurons expressing Esr1 (green). **(d)** Experimental schedule. **(e)** The percentage of VMHvl cells expressing light-induced c-Fos in the anterior vs. posterior VMHvl of all tested sites with over 10% of light induced c-Fos. **(f)** Representative raster plots illustrating progressive behavioral changes towards a female intruder with increased light intensity. **(g, h)** Increase in **(g)** duration of investigation and **(h)** duration of attack towards an adult female or male intruder during light-on period in comparison to sham-on period in animals with preferential posterior VMHvl activation. **(i)** The minimal light intensity that is required to elicit close investigation is lower than that to elicit attack against either a male or a female intruder. **(j)** The duration of investigation (left) and attacks (right) did not differ during light-on and sham-on periods in the control group. **g, h and j**, paired *t*-test; **i**, Two-way repeated measure ANOVA followed by Holm-Sidak post-hoc multiple comparisons; $^{*}p < 0.05$, $^{**}p < 0.01$, $^{***}p < 0.001$. Data are presented as means ± s.e.m.. [AU Query: OK?] See Supplementary Table 2 for detailed statistics. **See also** Supplementary Figure 7–10.

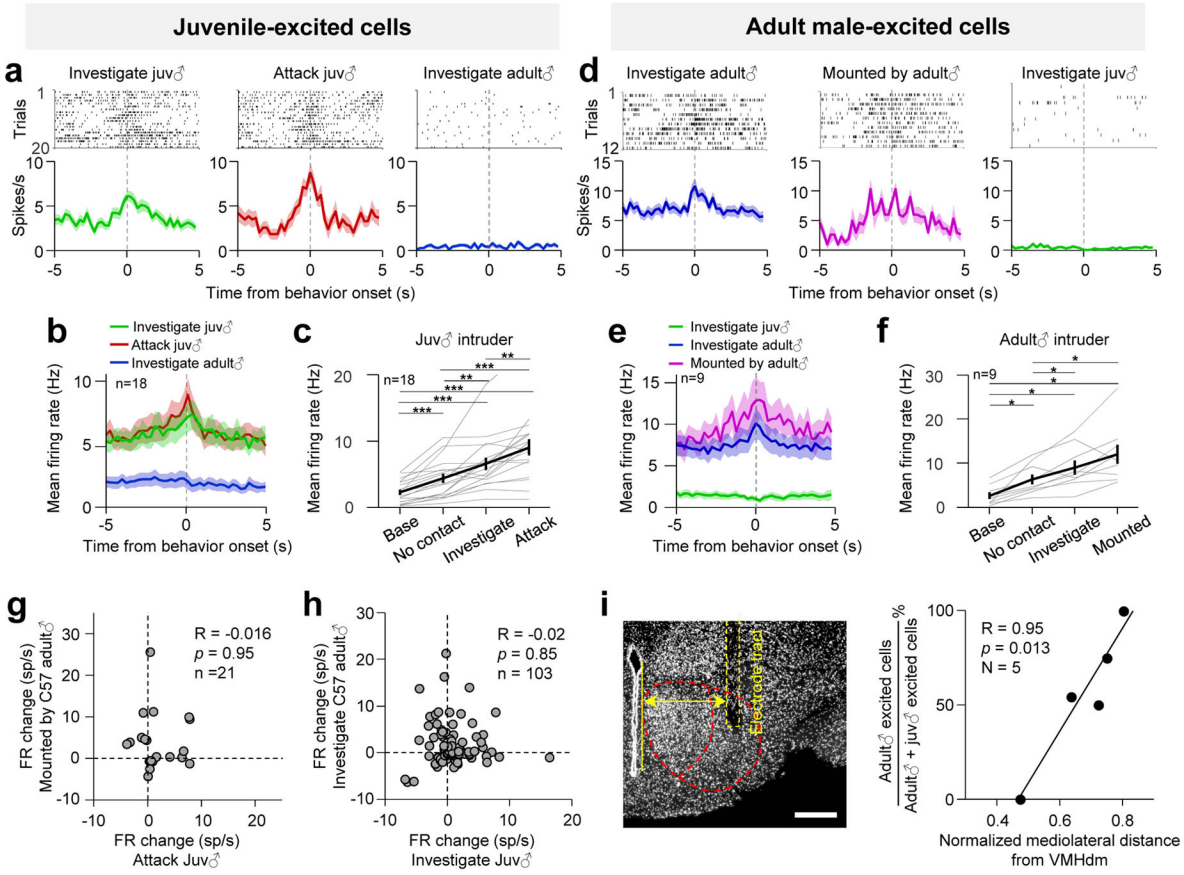

Figure 5. Electrophysiological responses of female VMHvl neurons during encounters with adult male and juvenile intruders

(a) Raster plots (top) and PETHs (bottom) aligned to the onsets of various behavioral episodes for a juvenile-excited cell. **(b)** Average PETHs of the firing rate from 18 juvenile-excited cells. **(c)** Firing rates of juvenile-excited cells before juvenile introduction (base) and when the animal investigated, attacked or stayed away from (no contact) the juvenile. **b and c** only show juvenile-excited cells with attacking juvenile episode. **(d)** Example and **(e–f)** population responses of adult male-excited cells. Figure conventions as in (**a–c**). **d–f** only show male-excited cells with being mounted episodes. **(g, h)** Distributions of the firing rate changes **(g)** during attack and being mounted or **(h)** during investigating juvenile and investigating an adult male across all the recorded cells with both behaviors. **(i)** Left, a representative histological image showing the electrode tract. Scale bar: 300 μm. Right, the correlation between mediolateral distance of the electrode and the percentage of recorded male-excited cells among all male-excited and juvenile-excited cells**. c, f:** One-way ANOVA followed by Holm-Sidak post-hoc multiple comparisons; **g, h, i**: Pearson product-moment correlation; $^{*}p < 0.05$, $^{**}p < 0.01$, $^{***}p < 0.001$. Data are presented as means ± s.e.m.. [AU Query: OK?] See Supplementary Table 2 for detailed statistics. **See also** Supplementary Figure 11.

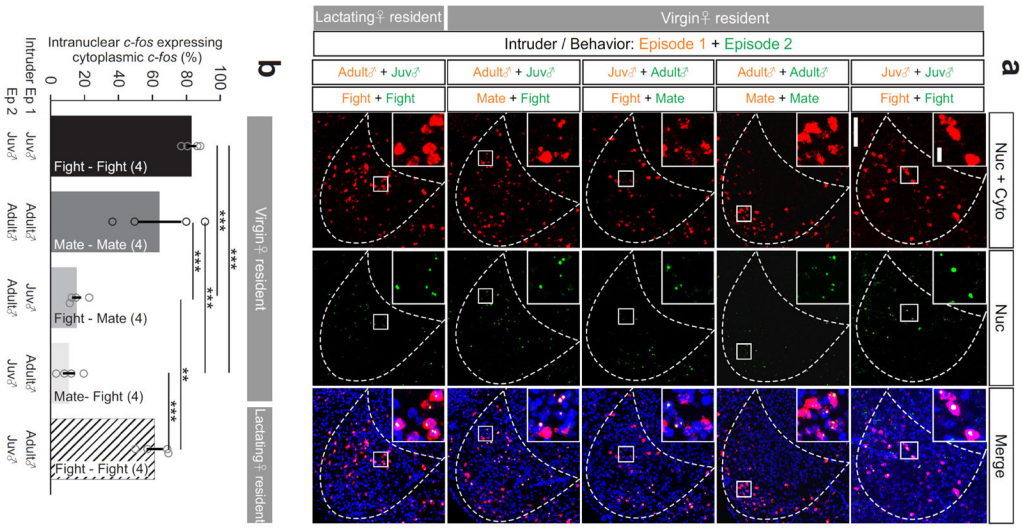

Figure 6. Topographical organization of fighting- and mating-related cells in the female VMHvl

(a) Cytoplasmic + nuclear (red) and nuclear only (green) *c-fos* induced by two sequential behavioral episodes. Insets show the enlarged images of the boxed areas. Blue: Hoechst. Scale bars: 150 μm and 20 μm (insets). **(b)** Percentage of neurons expressing nuclear *c-fos* that also express cytoplasmic *c-fos*. One-way ANOVA followed by Tukey's multiple comparisons. $^{**}p < 0.01$, $^{***}p < 0.001$. Data are presented as means ± s.e.m.. [AU Query: OK?] See Supplementary Table 2 for detailed statistics. **See also** Supplementary Figure 12.

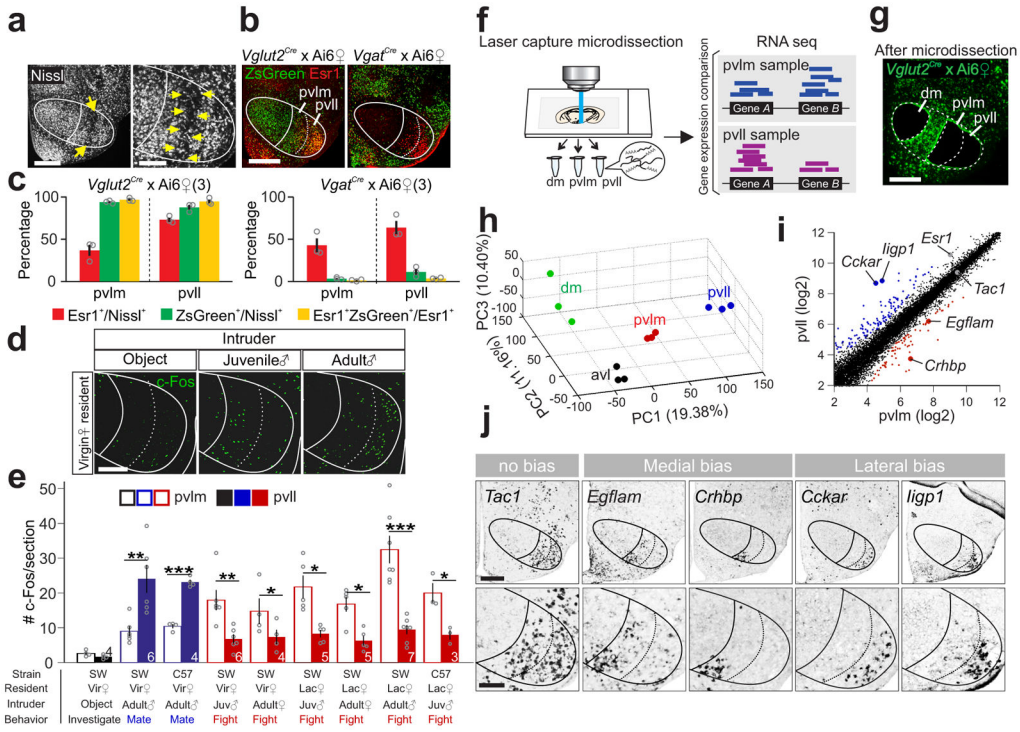

Figure 7. Female VMHvl has anatomically and molecularly distinct subdivisions

(a) Nissl staining illustrating the boundary (yellow arrows) between female VMHpvlm and VMHpvll. Scale bars (left and right): 300 and 150 μm. **(b)** Overlay of Esr1 (red) and ZsGreen (green) in the VMHvl of a female *Vglut2-ires-Cre* × Ai6 mouse (left) and a female *Vgat-ires-Cre* × Ai6 mouse (right). Scale bar: 300 μm. **(c)** The percentage of Esr1$^+$ (red), Vglut2$^+$ (green, left) and Vgat$^+$ (green, right) cells in the VMHpvll and VMHpvlm and the percentage of Esr1$^+$ cells that overlap with Vglut2$^+$ or Vgat$^+$ cells (yellow). (N = 3 animals for each group). **(d)** Object investigation, fighting or mating induced c-Fos (green) in the VMHvl in virgin female mice. Scale bar = 150 μm. **(e)** Average number of c-Fos$^+$ cells/section in the VMHpvlm and VMHpvll following object investigation (black), fighting (red) or mating (blue) in female mice. N = 3–7. paired *t*-test. *$p < 0.05$, **$p < 0.01$, ***$p < 0.001$. **(f)** Experimental scheme. **(g)** A brain section from a *Vglut2-ires-Cre* × Ai6 mouse after microdissection of VMHdm, VMHpvll and VMHpvlm. Scale bar: 300 μm. **(h)** RNAseq results of all samples from various VMHvl subregions mapped onto the principal component (PC) space. **(i)** Average normalized counts of each gene in the VMHpvlm (x-axis) and VMHpvll (y-axis). Red and blue dots represent genes with significantly biased expression (Benjamini and Hochberg method, $p < 0.05$, >1.2×, log2 scale). **(j)** In situs of 5 genes at the VMHvl that are indicated in **(i).** Scale bars (top and bottom): 300 and 150 μm. Data are presented as means ± s.e.m.. [AU Query: OK?] See Supplementary Table 2 for detailed statistics. **See also** Supplementary Figure 13.

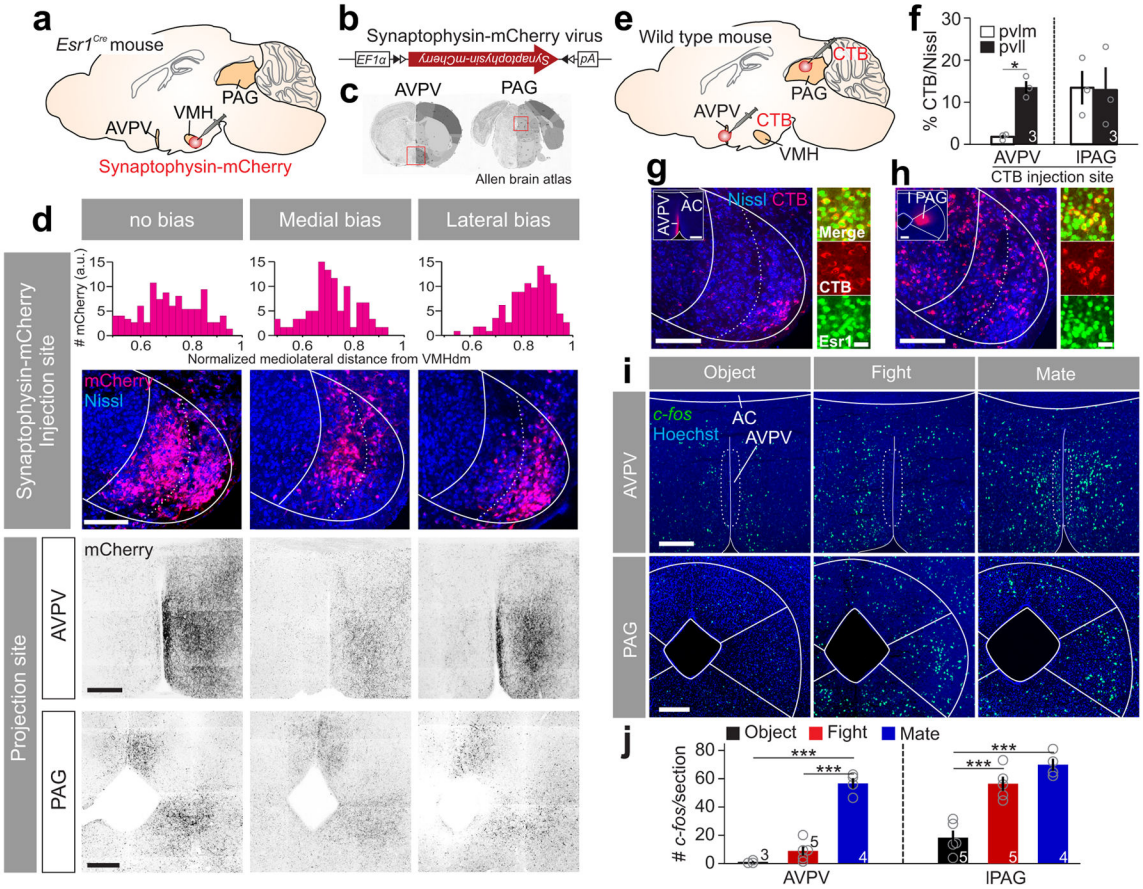

Figure 8. VMHpvlm and VMHpvll in female mice have distinct downstream targets

(a, b) Experimental scheme for anterograde tracing. **(c)** The two projection sites of the VMHvl (red boxes) that are shown in (**d**). Images from Allen Brain Atlas. **(d)** Projection patterns in the AVPV and PAG in animals with primary infection in the whole VMHvl (left), VMHpvlm (middle) and VMHpvll (right). Scale bars (top to bottom): 150, 300 and 300 μm. Top bar graphs show the distributions of infected neurons in the VMHvl along the medial-lateral axis. **(e)** Experimental scheme of retrograde tracing. **(f)** Percentage of neurons in the VMHplvm or VMHpvll that were retrogradely labeled from AVPV (left) or PAG (right). Paired *t*-test. $*p < 0.05$. **(g, h)** Left large image shows neurons in the VMHvl that are retrogradely labeled (red) from **(g)** AVPV or **(h)** PAG. Insets show the injection sites. Scale bars: 150 μm and 300 μm (insets); Right images show the overlap between the CTB labeling (red) and Esr1 (green). Scale bar: 20 μm. **(i)** *c-fos* mRNA expression in the AVPV or PAG after various testing conditions. Scale bars: 300 μm. **(j)** Average number of *c-fos* expressing cells per section in the AVPV (left) and PAG (right) after various testing conditions. One-way ANOVA followed by Tukey's multiple comparisons. $***p < 0.001$. Data are presented as means ± s.e.m. [AU Query: OK?] See Supplementary Table 2 for detailed statistics. **See also** Supplementary Figure 14.